

## Basis Independent Neutrino masses in the $R_p$ violating MSSM

---

**Sacha Davidson**

*Theoretical Physics, Oxford University, 1 Keble Road, Oxford, OX1 3NP, United Kingdom*

**Marta Losada**

*Centro de Investigaciones, Universidad Antonio Nariño, Cl. 59 No. 37-71, Santa Fe de Bogotá, Colombia*

**ABSTRACT:** We calculate the neutrino mass matrix up to one loop order in the MSSM without  $R$ -parity, including the bilinears in the mass insertion approximation. This introduces additional diagrams usually neglected in the literature. We systematically consider the possible new diagrams, and find a few missing from our previous work. We provide analytic expressions for the mass matrix elements in the neutrino flavour basis, which are independent of the  $H_d - L_i$  basis choice in the Lagrangian. We compare the contributions from different diagrams, and make “Lagrangian-basis-independent” estimates of when the new diagrams need to be included. We briefly discuss the phenomenology of a toy model of bilinear  $R$ -parity violation.

**KEYWORDS:** Neutrino Physics, Supersymmetric Standard Model, Solar and Atmospheric Neutrinos.

# 1. Introduction

The construction of a model which generates neutrino masses [1] requires some extension of the Standard Model. Supersymmetry [2, 3] is an interesting possibility which provides new (s)particles. We consider the Minimal Supersymmetric Standard Model (MSSM) without imposing  $R$ -parity. The quantum number  $R_p$  is defined as  $R_p = (-1)^{L+3B+2S}$ , where  $L$ ,  $B$ ,  $S$  are the lepton and baryon number and the spin of the particle, respectively [4]. In a general  $R_p$  non-conserving supersymmetric version of the SM, lepton number is not conserved<sup>1</sup>, which allows non-zero neutrino masses.

The main physical motivation for neutrino masses comes from the anomalous neutrino data from both solar and atmospheric neutrino experiments [5]. In the  $R$ -parity violating ( $\mathcal{R}_p$ ) MSSM, one neutrino can acquire a tree level mass through a see-saw effect from the mass matrix of the neutrinos and neutralinos [6]. In order that the rest of the neutrinos become massive, loop diagrams that violate lepton number (by two units) must also be considered [7, 8]. For the model to generate neutrino masses that fit experimental constraints we must require that:  $\Delta m_{\text{sun}}^2 \lesssim 10^{-4} \text{ eV}^2$ ,  $\Delta m_{\text{atm}}^2 \in [10^{-3}, 10^{-2}] \text{ eV}^2$ . For solar neutrino data there are several different possibilities for the relevant mixing angle (large or small mixing angle solutions) while for atmospheric neutrinos the mixing angle must be in the range  $\sin^2 2\theta_{\text{atm}} \in [0.85, 1]$ .

In the MSSM, the down-type Higgs and the lepton doublet superfields have the same gauge quantum numbers, which means that they can mix if lepton number is not conserved. Thus, we can construct a vector  $L_J = (H_d, L_i)$  with  $J : 4..1$ . With this notation, the superpotential for the supersymmetric SM with  $R_p$  violation can be written as

$$W = \mu^J H_u L_J + \frac{\lambda^{JK\ell}}{2} L_J L_K E_\ell^c + \lambda'^{Jpq} L_J Q_p D_q^c + h_t^{pq} H_u Q_p U_q^c. \quad (1.1)$$

We contract SU(2) doublets with  $\varepsilon_{\alpha\beta}$ :  $\varepsilon_{11} = \varepsilon_{22} = 0$ ,  $\varepsilon_{12} = -\varepsilon_{21} = -1$ . The  $R_p$  violating and conserving coupling constants have been assembled into vectors and matrices in  $L_J$  space: we call the usual  $\mu$  parameter  $\mu_4$ , and identify  $h_e^{jk} = \lambda^{4jk}$ <sup>2</sup> and  $h_d^{pq} = \lambda'^{4pq}$ . We call the usual  $\mathcal{R}_p$  mass  $\epsilon_i = \mu_i$ . Lower case roman indices  $i, j, k$  and  $p, q$  are lepton and quark generation indices. We frequently suppress the capitalised indices, writing  $\vec{\mu} = (\mu_4, \mu_3, \mu_2, \mu_1)$ . We also include possible  $R_p$  violating couplings among the soft SUSY breaking parameters, which can be written as

$$V_{\text{soft}} = \frac{\tilde{m}_u^2}{2} H_u^\dagger H_u + \frac{1}{2} L^{J\dagger} [\tilde{m}_L^2]_{JK} L^K + B^J H_u L_J \\ + A^{ups} H_u Q_p U_s^c + A^{Jps} L_J Q_p D_s^c + \frac{A^{JKl}}{2} L_J L_K E_l^c + h.c. \quad (1.2)$$

---

<sup>1</sup>Baryon number is also in general not conserved, however we will impose baryon number conservation by hand to avoid proton decay constraints, see *e.g.*, [9]

<sup>2</sup>We have changed convention with respect to factors of 2 in  $\lambda$  from our previous paper: we now put  $\lambda/2$  in the superpotential, with  $\lambda^{4ij} = h_e^{ij}$ .

Note that we have absorbed the superpotential parameters into the  $A$  and  $B$  terms; *e.g.* we write  $B^4 H_u H_d$  not  $B^4 \mu^4 H_u H_d$ . We abusively use capitals for superfields (as in eq. (1.1)) and for their scalar components.

In this notation where the Higgs joins the leptons as the fourth direction in  $\{L_I\}$  space, the relative magnitude of  $R_p$  violating and conserving coupling constants vary with the choice of the Higgs direction.  $R_p$  violation can be understood geometrically: if all interactions in the Lagrangian agree which direction is the Higgs (*e.g.*  $\hat{H} = \hat{L}_4$ ), then  $R_p$  is a good symmetry. But if there is misalignment in  $\{L_I\}$  space between different couplings constants (for instance  $\lambda^{'ipq} \neq 0$  in the basis where  $\mu_1 = \mu_2 = \mu_3 = 0$ ) then  $R_p$  is not conserved. This  $\mathcal{R}_p$  can be parametrised by basis independent combinations of coupling constants [6, 10, 11, 13]. These invariant measures of  $R_p$  violation in the Lagrangian are analogous to Jarlskog invariants which parametrise CP violation.

Early work on  $\mathcal{R}_p$  neutrino masses [7] used models where the bilinear  $\mathcal{R}_p$  could be rotated out of the mass terms ( $B_i, \mu_i, \tilde{m}_{4i}^2$ , referred to as “bilinears”) into the trilinear interactions. Most subsequent analytic estimates have followed the calculation of [7] and neglected the  $\mathcal{R}_p$  bilinear masses in the loop contributions to the neutrino masses. This does not generate the complete set of one loop diagrams contributing to  $[m_\nu]_{ij}$ , so it is formally inconsistent. It would be acceptable if neglecting the bilinear contributions corresponded to neglecting loops suppressed by some additional small parameter. However, the size of the bilinears is basis dependent, so what is neglected depends on the basis choice, and this basis dependence of neutrino masses has caused some confusion in the literature.

In a previous paper [12], we systematically analysed  $\Delta L = 2$  loop contributions to neutrino masses in the mass insertion approximation [14]. This led us to identify new diagrams which have not been included in many analytic estimates in the literature. We calculated the neutral loop diagram exactly (Grossman-Haber diagram), and gave basis-independent estimates for all diagrams using a common SUSY scale for all R-parity conserving mass parameters. The mass insertion approximation is valid as we know experimentally that neutrino masses are small. It is a particularly transparent way to include the bilinears, because the  $\mathcal{R}_p$  Feynman rules can be read off the Lagrangian, and all the  $\mathcal{R}_p$  appears perturbatively in the numerator (“upstairs”) of each contribution. The relative contributions of different diagrams are easy to see. The main point of our previous paper was that the issue of the basis choice for calculating neutrino masses is transparent if we keep all contributions.

The bilinear  $\mathcal{R}_p$  contribution to loops, as well as at tree level, has been included in [15, 16, 17], where neutrino masses are obtained, after the exact diagonalization of the mass matrices of all particles which propagate in the  $\Delta L = 2$  loops. The bilinears mix Standard Model and SUSY particles, generating mass matrices of large dimension, so these results are partially numerical. They propagate tree-level mass eigenstates in their loop diagrams. The discussion in ref. [17] includes gauge loops.

Reference [16] have approximate diagonalisation formulae, calculated in the seesaw approximation, which is equivalent to the mass insertion approximation used here; they have few diagrams and long mixing angle formulae, whereas we have more diagrams and only MSSM mixing angles.

The purpose of this paper is to provide basis-independent neutrino mass matrix elements, they are given in Appendices A and B. We present complete analytic expressions for all of the diagrams, and clarify how the neutrino mass matrix elements can be “basis-independent”. We discuss in detail when the different contributions to the neutrino mass matrix are relevant, identifying for both bilinear and trilinear contributions when they must be included or can be neglected. We discuss phenomenological issues for a toy model where the  $R_p$  violation comes from the soft SUSY breaking sector of the potential. In the literature, most analyses using neutrino data have taken into account only the effects of  $R_P$  violation from trilinears and the  $\mu$  bilinear [18].

In section 2, we discuss what we mean by “basis independent” neutrino mass matrix elements, what we calculate, and how basis dependent it is. In section 3, we discuss when the bilinears are important in the loop contributions to neutrino masses. This is a detailed discussion, with generation indices, of results presented in [12]. In section 4, we study the phenomenology of some simple bilinear models. We conclude in section 5. Exact one-loop neutrino mass matrix elements are presented in Appendix A in the  $\langle \tilde{\nu}_i \rangle = 0$  basis. In Appendix B, the neutrino mass matrix elements are given in terms of MSSM parameters and basis-independent combinations of coupling constants that parametrise  $\mathcal{R}_p$ . Additional Feynman rules for including  $\mathcal{R}_p$  in the mass insertion approximation can be found in Appendix C. Numerical bounds on R-parity violating parameters obtained from the different diagrams are given in Appendix D.

## 2. Issues of basis

There is no unique interaction eigenstate basis for the  $Y = -1$  fields (the components of the  $L_i$  and  $H_d$  superfields) in the  $\mathcal{R}_p$  MSSM. This means that the Lagrangian parameters depend on an arbitrary choice of basis, or equivalently that Lagrangians which differ by a rotation in  $\{L_I\}$  space make equivalent physical predictions. Observables cannot depend on the choice of basis in the Lagrangian  $\mathcal{L}$ , so they must be scalar functions of the vector and tensor parameters in  $\{L_I\}$  space. It is common in SUSY to study the dependence of physical observables on Lagrangian inputs. The basis-dependence of the Lagrangian makes this problematic in  $\mathcal{R}_p$  models because a point in physical parameter space corresponds to different numerical inputs in different bases. So comparing results calculated in different bases is difficult.

The  $\mathcal{R}_p$  in the Lagrangian can be parametrised in a basis independent way by combining coupling constants, masses and vacuum expectation values (vectors

and matrices in  $\{L_I\}$  space) into scalar “invariants”, which are zero when  $R_p$  is conserved. Physical observables can be expressed in terms of these invariants and other  $R_p$  conserving quantities. For a discussion of constructing invariants, see *e.g.* [10, 12, 13, 19].

Neutrino masses and mixing angles are measurable quantities, so must be (Lagrangian) basis-*independent*. The neutrino mass matrix  $[m_\nu]_{ij}$ ,  $i, j : 1..3$ , is basis *dependent*, depending on the choice of Higgs direction in  $\{L_I\}$  space, and on the choice of lepton flavour directions  $\hat{L}_i$  and  $\hat{L}_j$ . A physically motivated basis choice for the  $\hat{L}_i$  is the charged lepton mass eigenstate basis ( $\equiv$  the neutrino flavour basis), because the neutrino masses and mixing angles can be computed from  $[m_\nu]_{ij}$  in this basis, so it contains all the measurable information. We can express the charged lepton mass eigenstate vectors in a basis-independent way, using the mass insertion approximation, so we present *Lagrangian* basis independent expressions for the elements of  $[m_\nu]_{ij}$  in the flavour basis. So we have “basis-independent” expressions for matrix elements which are intrinsically basis-dependent—this is sensible because we want expressions which are independent of the arbitrary Lagrangian basis choice; the flavour basis is “physical”.

The basis we work in is

$$\begin{aligned} \hat{H}_d &= \frac{\vec{v}}{v} \\ \hat{L}^i &= \frac{\lambda^i \cdot \vec{v}}{|\lambda^i \cdot \vec{v}|}, \end{aligned} \quad (2.1)$$

where  $\vec{v}$  is the vector of vacuum expectation values in the down-type Higgs sector and we impose the requirement that  $\vec{v} \cdot \lambda^i \cdot \lambda^j \cdot \vec{v} \propto \delta^{ij}$ . The lower case index labelling the matrix  $\lambda^k$  is the singlet lepton index:  $[\lambda^k]_{IJ} = \lambda^{IJK}$ . So there are three flavour eigenstates  $\hat{L}^i$  in  $\{L_I\}$  space:  $\hat{L}_J^i = \lambda^{JKi} v_K / \sqrt{v_P \lambda^{NPi} \lambda^{NMi} v_M}$  (no sum on  $i$ )<sup>3</sup>. This corresponds to the charged lepton mass eigenstate basis in the absence of  $\mathcal{R}_p$ . In this  $R_p$  conserving case  $\lambda^{4ij} = h_e^{ij}$  and  $\lambda^{kij} = 0$ , where  $k, i, j : 1..3$ . So  $\lambda^{IJK} v_I = \sqrt{2} m_e^{jk}$  ( $I = 4, J = j : 1..3$ ),  $\vec{v} \cdot \lambda^i \cdot \lambda^j \cdot \vec{v} \propto \delta^{ij}$  is the condition that the  $\{e_R^c\}$  are in the mass eigenstate basis, and  $\lambda^i \cdot \vec{v}$  are the charged doublet eigenvectors. In the presence of bilinear  $\mathcal{R}_p$ , the basis (2.1) will not be exactly the charged lepton mass eigenstate basis. However, bilinear  $\mathcal{R}_p$  masses are required to be small by neutrino masses, so the basis (2.1) is close to the charged lepton mass eigenstate basis. We include the correction due to the bilinears in the mass insertion approximation.

Neutrino masses are proportional to  $\mathcal{R}_p$  couplings, and observed to be small. We can therefore compute neutrino masses by perturbing in  $\mathcal{R}_p$  masses and trilinear couplings. We include the bilinear  $\mathcal{R}_p$  masses in the mass insertion approximation, which means all  $\mathcal{R}_p$  couplings appear in the numerator (“upstairs”) of the expression

---

<sup>3</sup>The capitalised index ordering on  $\lambda^{NPi}$  is because  $\vec{a} \cdot \lambda \cdot \vec{b} = -\vec{b} \cdot \lambda \cdot \vec{a}$  is an antisymmetric product. The transpose of  $\hat{L}^i$  is  $-\vec{v} \cdot \lambda^i / |\vec{v} \cdot \lambda^i|$ .

$\delta_\mu^i \equiv \frac{\vec{\mu} \cdot \lambda^i \cdot \vec{v}}{ \vec{\mu}  \sqrt{2m_e^i}}$	$\frac{\mu^i}{ \mu }$
$\delta_B^i \equiv \frac{\vec{B} \cdot \lambda^i \cdot \vec{v}}{ \vec{B}  \sqrt{2m_e^i}}$	$\frac{B^i}{ B }$
$\delta_{\lambda'}^{ipq} \equiv \frac{\vec{\lambda}'^{pq} \cdot \lambda^i \cdot \vec{v}}{\sqrt{2m_e^i}}$	$\lambda'^{ipq}$
$\delta_\lambda^{ijk} \equiv \frac{\vec{v} \cdot \lambda^i \lambda^k \lambda^j \cdot \vec{v}}{2m_e^i m_e^j}$	$\lambda^{ijk}$

**Table 1:** The basis-independent invariants used to parametrise the  $\mathcal{R}_p$  relevant for neutrino masses, together with their value in the  $\langle \tilde{\nu}_i \rangle = 0$  basis. They are zero if  $R_p$  is conserved.  $\delta_\mu$  and  $\delta_B$  parametrise bilinear  $\mathcal{R}_p$ . Note that these invariants have signs: for arbitrary vectors  $\vec{a}$  and  $\vec{b}$ ,  $\vec{a} \cdot \lambda^i \cdot \vec{b} = -\vec{b} \cdot \lambda^i \cdot \vec{a}$ .

corresponding to a diagram. We propagate MSSM mass eigenstates, whose masses we make “basis-independent” by substituting  $B_4 \rightarrow \vec{B} \cdot \vec{v}/|\vec{v}|$ ,  $\mu_4 \rightarrow \vec{\mu} \cdot \vec{v}/|\vec{v}|$ , and  $\tilde{m}_{44}^2 \rightarrow \vec{v} \cdot \tilde{m}^2 \cdot \vec{v}/|\vec{v}|^2$ . The physically relevant flavour basis is written in terms of vevs and coupling constants (see equation 2.1), so neutrino mass matrix elements in this basis are proportional to invariants. We list the four invariants relevant for neutrino masses in table 2, along with their value in the basis where the sneutrinos have no vev.

A significant advantage of the basis-independent formalism is that the neutrino masses can be computed in any Lagrangian basis, including those where the mass insertion approximation is not valid. This could be easier than rotating to the  $\langle \tilde{\nu}_i \rangle = 0$  basis, because the vev is a derived quantity, calculated by minimising the potential. For instance, consider a model where all the  $\mathcal{R}_p$  is in  $\vec{B}$  and  $\vec{v}$ —that is, there is a basis where all the  $\mathcal{R}_p$  couplings other than  $B_i$  and  $\langle \tilde{\nu}_i \rangle$  are zero. Clearly it is easier to evaluate invariants in this basis than to rotate to  $\langle \tilde{\nu}_i \rangle = 0$ . The basis independent formalism also makes it simple to compare results computed in different bases.

The tree level neutrino mass is non-zero if  $\delta_\mu \neq 0$  [6]. The diagram appears in figure 1 in the mass insertion approximation. In the basis (2.1), it contributes a mass matrix

$$[m_\nu]_{ij}^{tree} = -(\vec{\mu} \cdot \hat{L}_i) \sum_\alpha \frac{Z_{\alpha 3}^* Z_{\alpha 3}^*}{m_{\chi_\alpha}} (\vec{\mu} \cdot \hat{L}_j), \quad (2.2)$$

which gives a mass  $m_3^{tree} = \sum_{i,\alpha} (\delta_\mu^i)^2 Z_{\alpha 3}^{*2} |\mu|^2 / m_{\chi_\alpha}$  to the neutrino

$$\hat{\nu}_3^{tree} = \frac{\delta_\mu^i}{\delta_\mu} \hat{L}_i, \quad (2.3)$$

where  $\delta_\mu = \sqrt{\sum_i (\delta_\mu^i)^2}$ , and the neutralino index  $\alpha$  runs from 1 to 4. The index “3” on  $Z$  corresponds to the interaction eigenstate  $\tilde{h}_u$ —see Appendix C for our conventions on  $Z$ . Equation (2.2) is equivalent to the usual formula  $m_\nu^{tree} = \det[M^{(5)}] / \det[M^{(4)}]$ , where  $M^{(5)}$  ( $M^{(4)}$ ) is the  $\mathcal{R}_p$   $5 \times 5$  neutralino and neutrino mass matrix (MSSM neutralino mass matrix), as can be seen by writing  $M^{(5)}$  and  $M^{(4)}$  in the MSSM mass eigenstate basis with  $\langle \tilde{\nu}_i \rangle = 0$ .

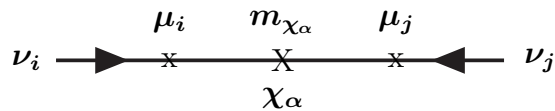


**Figure 1:** Tree-level neutrino mass in the mass insertion approximation

Loop corrections to the neutrino mass matrix can be divided into three categories. First, there are gauge and top Yukawa coupling loops which renormalise the mass of  $\nu_3^{tree}$ —we neglect these because their effect is small [15]. Secondly, there are loop corrections to  $\delta_\mu^i$  (equivalently,  $\mu_i$  and/or  $\langle \tilde{\nu}_i \rangle$ ) which can modify the direction of  $\hat{\nu}_3$ —these we include (they can be scale dependent, which we fix by setting  $Q^2 = m_{L_3}^2$ ). Finally, there are finite loops which give mass to any neutrino. The third group are the most interesting loops, because they generate mass for the remaining two neutrinos. Schematic representations of the one-loop neutrino mass diagrams that we consider are reproduced in figure 2. This is a slightly modified version of a figure from ref. [12]. Each of the four diagrams represents a number of Feynman diagrams. This should be an almost<sup>4</sup> complete set of one loop,  $\Delta L = 2$  diagrams which generate mass matrix elements for the neutrinos that are massless at tree level. The possible places on the diagram for the two required lepton number violating interactions are labelled *I..VIII*. With the definition  $\hat{H} \propto \vec{v}$ , lepton number violation is not possible at the charged lepton mass insertion in diagrams a) and d). (A sneutrino vev could provide lepton number violation at this point in a basis where  $\langle \tilde{\nu}_i \rangle \neq 0$ .)

In Appendix A, we list the loop diagrams, giving exact formulae in the  $\langle \tilde{\nu}_i \rangle = 0$  basis for each diagram’s contribution to  $[m_\nu]_{ij}$ . The basis-independent version of these formulae is in Appendix B. In table 2, we summarize the diagrams and make basis independent estimates by setting all the heavy masses to a unique scale  $m_{SUSY}$ . The lists starts with the canonical trilinear diagrams, then the Grossman-Haber loop

<sup>4</sup>We discuss in Appendix B why we neglect certain finite diagrams of the third type.

No.	diagram	position of $\mathbb{R}_p$	$16\pi^2 m_{SUSY} [m_\nu]^{ij}$
1	<i>a</i>	<i>II VII</i>	$\delta_\lambda^{ink} \delta_\lambda^{jkn} m_{e_n} m_{e_k}$
2	<i>b</i>	<i>II VII</i>	$3\delta_{\lambda'}^{iqq} \delta_{\lambda'}^{jqq} (m_{d_q})^2$
3	<i>c</i>	<i>IV VI</i>	$g^2 \delta_B^i \delta_B^j m_\chi m_{SUSY} / 4$
4	<i>b</i>	<i>I VII + II VIII</i>	$3(\delta_\mu^i \delta_{\lambda'}^{jq} + \delta_\mu^j \delta_{\lambda'}^{iqq}) (m_{d_q})^2 h_d^q$
5	<i>a</i>	<i>II VI</i>	$\delta_\lambda^{ijk} m_{e_k} \delta_B^k (m_{e_j} h_e^j - m_{e_i} h_e^i)$
6	<i>a</i>	<i>I VII + II VIII</i>	$(\delta_\mu^i \delta_\lambda^{jkk} + \delta_\mu^j \delta_\lambda^{ikk}) (m_{e_k})^2 h_e^k$
7	<i>a</i>	<i>I V</i>	$\delta_\mu^i \delta_\mu^j ((m_{e_j} h_e^j)^2 + (m_{e_i} h_e^i)^2)$
8	<i>a</i>	<i>II V</i>	$\delta_\lambda^{ijk} \delta_\mu^k m_{e_k} (h_e^i m_{e_i} - h_e^j m_{e_j})$
9	<i>a</i>	<i>III V</i>	$\delta_\mu^i \delta_\mu^j m_{e_j} m_{e_i} h_e^i h_e^j$
10	<i>a</i>	<i>III VIII</i>	$\delta_\mu^i \delta_\mu^j ((m_{e_i} h_e^i)^2 + (m_{e_j} h_e^j)^2)$
11	<i>a</i>	<i>I VI</i>	$\delta_\mu^i \delta_B^j (m_{e_j} h_e^j)^2 + \delta_\mu^j \delta_B^i (m_{e_i} h_e^i)^2$
12	<i>a</i>	<i>III VII</i>	$\delta_\lambda^{ijn} \delta_\mu^n m_{e_n} (m_{e_j} h_e^j - m_{e_i} h_e^i)$
13	<i>a</i>	<i>III VI</i>	$(\delta_B^i \delta_\mu^j h_e^j h_e^i m_{e_i} m_{e_j} + \delta_B^j \delta_\mu^i h_e^i h_e^j m_{e_j} m_{e_i})$
14	<i>d</i>	<i>III IV</i>	$g(\delta_B^i \delta_\mu^j (m_{e_j})^2 + \delta_B^j \delta_\mu^i (m_{e_i})^2)$
15	<i>d</i>	<i>III VIII</i>	$g\delta_\mu^i \delta_\mu^j ((m_{e_i})^2 + (m_{e_j})^2)$
16	<i>d</i>	<i>I III</i>	$g\delta_\mu^i \delta_\mu^j ((m_{e_i})^2 + (m_{e_j})^2)$
17	<i>d</i>	<i>I VII</i>	$gm_{e_k} m_{SUSY} (\delta_\mu^i \delta_\lambda^{jkk} + \delta_\mu^j \delta_\lambda^{ikk})$ $3gm_{d_k} m_{SUSY} (\delta_\mu^i \delta_{\lambda'}^{jkk} + \delta_\mu^j \delta_{\lambda'}^{ikk})$
18	<i>d</i>	<i>III VII</i>	zero for degenerate sleptons
19	<i>c</i>	<i>I VI + IV VIII</i>	$g^2 m_{SUSY}^2 (\delta_B^i \delta_\mu^j + \delta_\mu^i \delta_B^j) / 4$
20	<i>d</i>	<i>I V</i>	$g\delta_\mu^i \delta_\mu^j ((m_{e_i})^2 + (m_{e_j})^2)$
21	<i>d</i>	<i>I IV</i>	$g(\delta_\mu^i \delta_B^j (m_{e_j})^2 + \delta_\mu^j \delta_B^i (m_{e_i})^2)$

**Table 2:** Estimated contributions to  $[m_\nu]^{ij}$  from all the diagrams. In the second two columns is the label of the diagram of figure 2, and the position on the diagram of the two  $\Delta L = 1$  interactions. Column four is the “basis independent” estimated contribution to the neutrino mass matrix in the flavour basis. All indices other than  $i$  and  $j$  are summed.

induced by the soft bilinears, and finally all the additional diagrams which arise when the bilinear  $\delta_\mu^i$  are included in the loops. For each diagram, labelled by  $a \rightarrow d$  for the diagram category of figure 2, and by roman numeral identifying where the  $\mathbb{R}_p$  should appear on the figure, we give an estimate of the diagram in terms of the invariants listed in table 1. We have added a few relevant diagrams missing from the original list. In Appendix B, we make an exhaustive list of all potential diagrams, explain why some are zero, and give basis-independent expressions.

To evaluate diagram b) with  $\mathbb{R}_p$  at points *II* and *VII* (this is the usual coloured trilinear diagram), we identify the external neutrino legs as  $\hat{L}_i$  and  $\hat{L}_j$ . At vertices *II* and *VII* sit couplings  $\vec{\lambda}'^{sp}$  and  $\vec{\lambda}'^{rs}$ . (The bold face indices correspond to the

squark mass eigenstate basis—see Appendix C.) The diagram is therefore

$$\begin{aligned}
[m_\nu]_{kj} &= -3 \sum_{s,\mathbf{p},\mathbf{r}} (i\hat{L}_k \cdot \vec{\lambda}'^{s\mathbf{p}})(i\vec{\lambda}'^{rs} \cdot \hat{L}_j)(i|\tilde{A}_d^{\mathbf{pr}}|)(-|m_{d_s}|) \\
&\quad \times \int \frac{d^4k}{(2\pi)^4} \frac{i}{k^2 - m_{\tilde{D}_p}^2} \frac{i}{k^2 - m_{\tilde{Q}_r}^2} \frac{i}{k^2 - m_{d_s}^2} + (k \leftrightarrow j) \\
&= -\frac{3}{16\pi^2} \sum_{s,\mathbf{p},\mathbf{r}} \lambda'^{k s \mathbf{p}} \lambda'^{j r s} \lambda'^{M s s} \frac{v_M}{\sqrt{2}} \left[ (\lambda A)'_{R\mathbf{r}\mathbf{p}} \frac{v_R}{\sqrt{2}} \right. \\
&\quad \left. + \frac{v_u}{\sqrt{2}} \mu_R \lambda'^{R\mathbf{r}\mathbf{p}} \right] I(m_{\tilde{Q}_r}, m_{\tilde{D}_p}, m_{d_s}) + (k \leftrightarrow j) \\
&= -\frac{3}{16\pi^2} \sum_{s,\mathbf{p},\mathbf{r}} \delta_{\lambda'}^{k s \mathbf{p}} \delta_{\lambda'}^{j r s} I(m_{\tilde{Q}_r}, m_{\tilde{D}_p}, m_{d_s}) |\tilde{A}_d^{\mathbf{pr}}| |m_{d_s}| + (k \leftrightarrow j) \quad (2.4)
\end{aligned}$$

$$\sim -\frac{3\delta_{\lambda'}^{k s \mathbf{p}} \delta_{\lambda'}^{j r s} |m_{d_s} m_{d_p}|}{8\pi^2 m_{SUSY}}, \quad (2.5)$$

$$(2.6)$$

where  $\tilde{A}^{\mathbf{pr}} = -[(A\lambda')^{R\mathbf{p}\mathbf{r}} v_R + v_u \mu_R \lambda'^{R\mathbf{p}\mathbf{r}}]$ , and we work in the down quark mass eigenstate basis:  $\vec{\lambda}'^{st} \cdot \vec{v}$  is diagonal. The integrals  $I$  are listed in Appendix A. The last line corresponds to the last column of table 2. Note that we do not divide by 2 when we symmetrise on  $i$  and  $j$ , because the diagram with  $i \leftrightarrow j$  is different. This agrees with [16, 17]<sup>5</sup> and disagrees with [8]. It is clear in the mass insertion approximation that one should not divide by 2, because in one case  $\nu_i$  couples to  $\tilde{D}^c$  and in the other case to  $\tilde{Q}$ . In the mass eigenstate formalism, one can see that these are distinct diagrams not included in the sum over  $p, r, s$  by considering the case where only  $\lambda'^{132}$  and  $\lambda'^{223}$  are non-zero.

In our previous paper, we were unclear about whether the charged goldstone boson of SU(2) could mix with the  $\{E^c\}$ . This was due to various sign discrepancies in the literature. As expected, the goldstone is pure SU(2)—so there is no loop diagram propagating a  $W^\mu$  that is proportional to a gauge times a Yukawa coupling.

### 3. When are the bilinears important in loops?

Bilinear contributions to loops have traditionally been neglected, which intuitively seems reasonable if they are “small” in a “sensible” basis close to the MSSM. However, this apparently reasonable oversight is confusing, because the size of what is neglected depends on the basis choice. In this section, we provide basis-independent conditions for when the bilinears can be neglected in the loops—assuming the mass matrix elements are then calculated in a sensible basis where the bilinears are small. These are not hard and fast rules, but estimates of when the extra bilinear diagrams should be included.

<sup>5</sup>We thank E.J. Chun for a discussion of this point.

A slightly different approach would be to consider the relative size of all the diagrams, and catalogue all the permutations of which diagrams should be included and which neglected. For instance, it is possible that the trilinears are negligible with respect to the bilinear diagrams, or that the  $\lambda$  trilinear contributes only a small correction to the  $\lambda'$  trilinear, and can be ignored. Here we assume that the trilinear contributions are always calculated, because they take little effort. Then we ask whether  $\delta_B$  should also be included—this is a few more diagrams. Finally we consider adding the  $\delta_\mu$  contributions, which is many more diagrams. We do not specifically discuss the case where  $\delta_\mu$  should be included but the  $\delta_B$  contributions are insignificant, because the  $\delta_B$  diagrams are relatively little work compared to the many  $\delta_\mu$  diagrams.

In our previous paper, we outlined three cases:

- **A:** all the bilinear contributions to loop diagrams are negligible. In this case the loop contributions to the neutrino mass matrix are the usual trilinear diagrams of figures 2a and 2b.
- **B:**  $\delta_\mu$  is negligibly small, but  $\delta_B$  should be included. In addition to the diagrams of case A, one should consider the neutral Grossman-Haber loop of figure 2c, and possibly the  $\delta_B$  mass insertion to figure 2a.
- **C:** Include all bilinear  $\mathcal{R}_p$  contributions. There are additional contributions to diagrams 2a, 2b, and 2c, and a new diagram 2d.

We determine basis-independent criteria for when the bilinears can be neglected in the loops by comparing our estimates of the size of each diagram from the last column of table 2. A diagram should be included if its contribution is of order the trilinear loops—however, we want to avoid comparing bilinear loop corrections of the tree mass (which are irrelevant), with the trilinear loops contributing masses to neutrinos which are massless at tree level. So we distinguish two cases:  $m^{tree} \lesssim m^{loop}$ , and  $m^{tree} \gg m^{loop}$ .

If  $m^{tree} \lesssim m^{loop}$ , we simply compare bilinear to trilinear loop mass matrix elements. Since  $\delta_\mu^i$  is not large enough to produce  $m^{tree} \gtrsim m_{ij}^{loop}$ , it is negligible in the loops, so we are in cases A or B.

If  $m^{tree} \gg m^{loop}$ , we consider only the loop mass matrix for the neutrinos that are massless at tree level. We compare the bilinear and trilinear contributions to this sub-matrix. Cases A, B, or C can arise if  $m_3^{tree} \gg m^{loop}$ .

### 3.1 case B—including the soft bilinear $B_i$

We first consider when  $\delta_B$  should be included in the loops. The Grossman-Haber loop is of order<sup>6</sup>  $m_\nu^{ij} \sim g^2 \delta_B^i \delta_B^j m_\chi / (64\pi^2)$ , which is potentially large because it is pro-

<sup>6</sup>We are neglecting flavour violation among the sneutrinos, which could induce a significant loop mass even if  $\vec{B} \simeq b\vec{\mu}$  [23].

portional to gauge rather than Yukawa couplings. Recall that the canonical trilinear diagrams are of order  $m_\nu^{ij} \sim \delta_{\lambda'}^{i33} \delta_{\lambda'}^{j33} m_b^2 / (8\pi^2 m_{SUSY})$ .

If the tree mass is small,  $m^{tree} \lesssim m^{loop}$ , then the Grossman-Haber loop should be included if it is of order the trilinear loop. This will occur if

$$\frac{g}{2} \delta_B^j \gtrsim \delta_{\lambda'}^{jqp} \sqrt{h_d^q h_d^p}, \quad \delta_\lambda^{jkl} \sqrt{h_e^k h_e^l}, \quad (3.1)$$

or the condition to neglect  $\delta_B$  can be roughly estimated as

$$\delta_B^j \ll \delta_{\lambda'}^{j33} h_b, \delta_\lambda^{j33} h_\tau \quad (m^{tree} \lesssim m^{loop}), \quad (3.2)$$

Alternatively, if  $m^{tree} \gg m^{loop}$ , we are only interested in the loop contributions to the mass of neutrinos  $\nu_2$  and  $\nu_1$  who are massless at tree level: if  $\vec{B}$  is aligned with  $\vec{\mu}$ , then the GH loop is a correction to the tree-level mass, and can be neglected along with other such loops.  $\vec{B}$  can be decomposed in components parallel and perpendicular to  $\mu$ :

$$\vec{B} = \vec{B}_\perp + \vec{B}_\parallel, \quad (3.3)$$

with  $\vec{B}_\parallel = (\vec{B} \cdot \vec{\mu}) \vec{\mu} / |\vec{\mu}|^2$ . The part of the Grossman-Haber loop proportional to  $\delta_{B_\parallel}^i \delta_{B_\parallel}^j$  is a loop correction to the tree mass  $m^{tree}$ . The  $\delta_{B_\parallel}^i \delta_{B_\perp}^j$  terms mix  $\nu^{tree}$  with  $\nu_2$  and  $\nu_1$ , and the mass matrix from the GH loop for  $\nu_1$  and  $\nu_2$  is

$$[m_\nu]_{ij} \propto \frac{\delta_{B_\perp}^i \delta_{B_\perp}^j}{64\pi^2} m_\chi. \quad (3.4)$$

This will be comparable or greater than the trilinear loops when

$$\frac{g}{2} \delta_{B_\perp}^i = \frac{g}{2} (\delta_B^i - \frac{\vec{B} \cdot \vec{\mu}}{|\vec{B}| |\vec{\mu}|} \delta_\mu^i) \gtrsim \delta_{\lambda'_\perp}^{jqp} \sqrt{h_d^q h_d^p}, \quad \delta_\lambda^{jkl} \sqrt{h_e^k h_e^l}. \quad (3.5)$$

We define  $\delta_{\lambda'_\perp}^{jqp} = \delta_{\lambda'}^{jqp} - \delta_\mu^j (\vec{\lambda}'^{qp} \cdot \vec{\mu}) / |\vec{\mu}|$ . This translates roughly into the condition that  $\delta_B$  can be neglected in the loops if

$$\delta_{B_\perp}^i \ll \delta_{\lambda'_\perp}^{i33} h_b, \delta_\lambda^{i33} h_\tau \quad (m^{tree} \gg m^{loop}). \quad (3.6)$$

### 3.2 case C—including $\mu_i$

The tree-level neutrino mass is  $\sim \sum_i (\delta_\mu^i)^2 m_\chi$ , so if  $\delta_\mu^i$  is relevant in the loops, then  $m^{loop} \ll m^{tree}$ . The additional diagrams proportional to  $\delta_\mu^i$  should be included if they induce a loop mass for  $\nu_2$  and  $\nu_1$  greater than or of order the trilinear or GH loops.

We first consider the various  $\delta_\mu^i$  contributions to diagrams *a* and *d* of figure 2 which are of order  $\sim [\delta_\mu^i (h_e^i)^2] [\delta_\mu^j (h_e^j)^2] m_{SUSY}$ . Generically the vector  $(\delta_\mu^\tau h^\tau h^\tau, \delta_\mu^\mu h^\mu h^\mu, \delta_\mu^e h^e h^e)$  will not be aligned with  $(\delta_\mu^\tau, \delta_\mu^\mu, \delta_\mu^e)$ , so the  $\delta_\mu$  bilinear contributions should be included if

$$\delta_\mu^i (h_e^i)^2 \gtrsim \delta_\lambda^{jkl} \sqrt{h_e^k h_e^l}, \delta_{\lambda'_\perp}^{jpq} \sqrt{h_d^p h_d^q}, \quad i, j, k, l, p, q \text{ not summed.} \quad (3.7)$$

A rough guide to when these  $\delta_\mu$  corrections can be neglected is therefore

$$\delta_\mu^j h^\tau \ll \delta_\lambda^{i\tau\tau}, \delta_{\lambda_\perp}^{i33} \left( \frac{h_b}{h_\tau} \right). \quad (3.8)$$

There are also bilinear loop contributions of the form

$$[m^{loop}]_{ij} \sim [\delta_\mu^i (h_e^i)^2] [\delta_\mu^j] m_{SUSY} \quad (i, j \in \{\tau, \mu, e\}). \quad (3.9)$$

These initially appear more significant, because they are only suppressed by two, rather than four, trilinears or yukawas. However,  $m_\nu^{loop} \ll m_\nu^{tree}$  and  $\hat{\nu}^{tree} \propto (\delta_\mu^\tau, \delta_\mu^\mu, \delta_\mu^e)$ , so contributions of the form of equation (3.9) mix  $\hat{\nu}^{tree}$  with  $\nu^2$  and  $\nu^1$ . These latter two neutrinos, which are massless at tree level, therefore acquire a seesaw mass of order

$$\begin{aligned} [m^{loop}]_{ij} &\sim \sum_k \delta_\mu^i (h_e^i)^2 m_{SUSY} \frac{(\delta_\mu^k)^2}{|\delta_\mu|^2 m_{SUSY}} (h_e^j)^2 \delta_\mu^j m_{SUSY} \\ &\sim [\delta_\mu^i (h_e^i)^2] [(h_e^j)^2 \delta_\mu^j] m_{SUSY} \quad (i, j \in \{3, 2, 1\}). \end{aligned} \quad (3.10)$$

This is the mass matrix structure we considered before equation (3.7), and will make a significant contribution if equation (3.7) is satisfied. So equation (3.7) is the condition for when  $\delta_\mu$  bilinears should be included in loops, or equivalently, equation (3.8) is a rough estimate of when the  $\delta_\mu$  loops can be neglected.

## 4. Phenomenology

In this section we briefly consider the constraints that can be set on  $\mathcal{R}_p$  couplings from solar and atmospheric neutrino data. We follow the approach of [20, 21], who set bounds on  $\mathcal{R}_p$  models corresponding to case A—models where the bilinears are negligible in loops and neutrino loop masses are due to trilinear couplings. We discuss here a toy model where the  $\mathcal{R}_p$  is in the bilinears, and the  $\delta_B$  loops make a significant contribution to  $[m_\nu]_{ij}$  (case B of the previous section). We leave case C—where  $\delta_\mu$  should be included in the loops—for a subsequent analysis [24]. We would like to establish bounds on the different set of basis independent combinations of coupling constants that contribute to the neutrino mass matrix. These bounds are more indicative of orders of magnitude than steadfast constraints. In order to proceed we make the following assumptions. First, we use the results of reference [20], which constrain a general  $3 \times 3$  symmetric mass matrix from neutrino data considering: atmospheric and solar neutrino experiments, CHOOZ experiment and the constraint from neutrinoless double beta decay. The overall conclusion of this analysis is that the mass matrix elements should be constrained to be on the order of  $|[m_\nu]_{ij}| \lesssim 0.1\text{eV}$ . Here we present our bounds allowing each individual matrix element to take on the maximum value of 0.1 eV. This simple approach can be

extended to obtain bounds when we include combinations of contributions to the neutrino mass matrix from  $\delta_\mu^i$ ,  $\delta_B^i$ ,  $\delta_\lambda^{ijk}$ , for any given model which contains these R-parity violating terms originally in the Lagrangian.

Secondly, we assume that each of the contributions from the diagrams that we have found is separately the unique contribution at a given time<sup>7</sup>. In this way we are trying to obtain the *weakest* constraint on the basis-independent combination of coupling constants. That is we allow each separate contribution to take on its maximum value. We can then choose from all of the bounds which is the strongest constraint on a given combinations of coupling constants. We also assume, unless otherwise indicated, that all supersymmetric mass scales are the same of order  $m_{susy}$ . The next approximation we make is that when we sum over neutralinos or charginos there is no suppression arising from the mixing angles<sup>8</sup>. We also assume that the magnitude of all R-parity violating couplings constants to be generation blind separately. That is, all  $B_i$  to be of the same order of magnitude, and similarly for  $\mu_i$ ,  $\lambda_{ijk}$ ,  $\lambda'_{ijk}$ , but we do not suppose beforehand that R-parity violating coupling constants arising from different terms in the Lagrangian are also of the same order of magnitude. The numerical results for all diagrams are summarized in appendix D.

As we can see from the tables in appendix D the strongest bounds for the combination of basis-independent coupling constants  $\delta_B^i \delta_B^j$  arises from the Grossman-Haber diagram:

$$\delta_B^i \delta_B^j < 3 \times 10^{-10} \quad . \quad (4.1)$$

For  $\delta_B^i \delta_\mu^j$  the best bound comes from diagram 19, which is the neutral Grossman-Haber loop with R-parity violation at points I and VI:

$$\delta_B^i \delta_\mu^j < 7 \times 10^{-10} \quad . \quad (4.2)$$

(We use  $\tan \beta = 2$  and a generic  $m_{susy} \sim 100$  GeV for both these bounds.) The strongest constraint on  $\delta_\mu^i \delta_\mu^j$  is from the tree-level mass:

$$\delta_\mu^i \delta_\mu^j < 10^{-12} \quad . \quad (4.3)$$

For comparison, we list the bounds which can be derived from the remaining diagrams in Appendix D.

#### 4.1 Toy Model

Suppose we only allow the presence of the basis-independent combinations of coupling constants  $\delta_\mu^i$  and  $\delta_B^i$ . A non-zero value of  $\delta_\mu^i$  can arise either from having  $\mu_i \neq 0$  or  $\langle \tilde{\nu}_i \rangle \neq 0$ , so this model could arise if all the  $\mathcal{R}_p$  originates in the soft SUSY breaking terms  $B_i$ , which induces a misalignment between the vev and superpotential

---

<sup>7</sup>This may be incorrect in a poorly chosen basis, where different diagrams cancel each other [24].

<sup>8</sup>We leave a further analysis of this aspect to future work.

couplings. (This would induce  $\delta_\lambda \sim h_b \delta_\mu$  and  $\delta_\lambda \sim h_\tau \delta_\mu$ , which we neglect because we assume our model to be in case B, where contributions of this size can be neglected.) This differs slightly from the usual bilinear model, discussed in detail in [15, 16, 17], where the  $\vec{R}_p$  originates in the GUT-scale misalignment between  $\vec{\mu}$  and the trilinears, so that  $\vec{B}$  becomes misaligned with respect to  $\vec{\mu}$  while running down to the weak scale. From the results of appendix D, we see that the relevant contributions to the neutrino mass matrix will arise from the tree level contribution plus diagrams 3 and 19. The upper bound  $\delta_\mu^i \lesssim 10^{-6}$  from the tree level mass contribution ensures that (for low  $\tan \beta$ ) the remaining diagrams, which in principle contribute to the neutrino mass matrix through mass insertions of  $\delta_\mu^i$  in the loops, are negligible.

With these three contributions we can obtain neutrino masses in the phenomenologically interesting region which can simultaneously satisfy atmospheric and solar neutrino data constraints. There are several ways to see this. The full mass matrix using our simple approximations is given by,

$$m_\nu^{ij} = m_{\text{susy}} \delta_\mu^i \delta_\mu^j + a_1 m_{\text{susy}} \delta_B^i \delta_B^j + a_1 m_{\text{susy}} (\delta_B^i \delta_\mu^j + \delta_B^j \delta_\mu^i), \quad (4.4)$$

where  $a_1 \simeq \frac{g^2}{64\pi^2}$ . Certain subcases of this mass matrix can generate neutrino mass textures, which have been analyzed in the literature, that can produce neutrino masses and mixing angles in accordance with present neutrino data. As a simple example, we see that if we set  $\delta_B^3 = 0$ , the structure of the neutrino mass matrix corresponds to the one analysed in case 1 of ref. [21]. In this case the neutrino mass matrix at one-loop consists simply of the tree-level term plus a correction to the 1-2 submatrix. The subcase analyzed in ref. [21] had this same structure but the loop correction was due to the trilinear diagram.

It is well known that the tree level contribution can give mass to only one of the neutrinos. Together with the loop contributions one of the neutrinos will have a mass

$$m_{\nu^3} = m_{\text{susy}} \sum_i |\delta_\mu^i + \sqrt{a_1} \delta_{B\parallel}^i|^2, \quad (4.5)$$

where we have used the decomposition  $\vec{B} = \vec{B}_\perp + \vec{B}_\parallel$  of equation (3.3).

The sub-mass-matrix for the remaining two neutrinos  $\nu^1$  and  $\nu^2$  is given by

$$m_\nu^{ij} = a_1 m_{\text{susy}} \delta_{B_\perp}^i \delta_{B_\perp}^j. \quad (4.6)$$

Terms of the form  $\delta_{B_\perp}^i \delta_\mu^i$  mix the heavier  $\nu^3$  and the lighter ( $\nu^1, \nu^2$ ). It can be seen from equation (3.10) that the seesaw mass generated from this mixing is suppressed, given our choice of SUSY parameters, compared to the direct loop contribution given in eq. (4.6).

This simple example <sup>9</sup> shows that a hierarchical neutrino mass spectrum, which satisfies atmospheric and solar neutrino data constraints, can easily be obtained by

---

<sup>9</sup>We leave a more detailed numerical analysis for future work.

taking  $|\delta_\mu + \sqrt{a_1}\delta_{B_\parallel}| \sim \text{few} \times 10^{-6}$  and  $\delta_{B_\perp}^i \sim \text{few} \times 10^{-6} - 10^{-5}$ . This gives us a massless neutrino and two massive neutrinos such that  $\Delta m_{atm} \sim m_{\nu^2_3}^2$  and  $\Delta m_{solar} \sim m_{\nu^2_2}$ . It is also possible to obtain other types of spectra for different input values.

## 5. Conclusions

There are many diagrams which can contribute to the neutrino mass matrix in the framework of the MSSM without R-parity. In general, in the literature only a few of these have been considered. In the present paper we have obtained the full analytic expression for the different diagrams contributing to the neutrino mass matrix from R-parity violating bilinear and trilinear coupling constants. We have expressed each contribution both in the  $\langle \tilde{\nu}_i \rangle = 0$  basis and in terms basis-independent combinations of couplings. We have also shown when the separate diagrams should be included/are relevant in the context of a given consistent framework. We have presented bounds on combinations of the basis-independent couplings constants from neutrino experimental data, and shown that a simple toy model of bilinear R-parity violation can successfully accommodate the necessary mass squared differences to account for the neutrino oscillations.

## Acknowledgements

We would like to thank Eung Jin Chun, Herbi Dreiner and Paolo Gambino for useful conversations. The work of M.L. was partially supported by Colciencias-BID, under contract no. 120-2000.

## Appendices

In these Appendices, we present the one loop contributions to the neutrino mass matrix, *excluding* the one-loop corrections to the mass of  $\hat{\nu}_3$ , the eigenstate that acquired mass at tree level. So we will consistently neglect loops with  $\mathcal{R}_p$  at I and VIII. We are interested in the one-loop masses for the neutrinos that are massless at tree level. In a subsequent publication, we will extract these from our results and discuss their phenomenology. Notice that these contributions are a subset of the loops we present here, because the direction of the eigenvector  $\hat{\nu}_3$  changes at one-loop: we neglected here the loop corrections to the mass of  $\hat{\nu}_3^{tree}$ , but included loops which change the direction of  $\hat{\nu}_3$  from  $\hat{\nu}_3^{tree} \rightarrow \hat{\nu}_3^{tree+loop}$ .

In Appendix A, we list diagrams in the order of the table 2. We give the amplitude for each non-zero diagram in the  $\langle \tilde{\nu}_i \rangle = 0$  basis. We impose  $\langle \tilde{\nu}_i \rangle = 0$  at one loop, setting  $Q^2 = m_{L_3}^2$  in the one-loop minimisation conditions, which can be found

in ref. [19]. In Appendix B, we systematically list all diagrams, ordering them by the roman numerals that identify in figure 2 where are the two units of  $\mathcal{R}_p$ . The amplitudes in Appendix B are “basis-independent”, that is they are expressed in terms of invariants and MSSM parameters. Notice that the neutrino mass matrix elements are *minus* the amplitude for the diagram,  $[m_\nu]_{ij} = -\mathcal{M}_{ij}(p^2 = 0)$ , so our formulae are for  $-[m_\nu]_{ij}$ . We present the  $\mathcal{R}_p$  Feynman rules in Appendix C. Appendix D contains our numerical results for bounds placed on combinations of basis-independent couplings constants from neutrino data.

## A. Diagrams in $\langle \tilde{\nu}_i \rangle = 0$ basis

We define

$$\tilde{A}^{\mathbf{ml}} = -\left( (h_e A)^{\mathbf{ml}} \frac{v_d}{\sqrt{2}} + \mu \frac{v_u}{\sqrt{2}} h_e^{\mathbf{ml}} \right), \quad (\text{A.1})$$

and

$$\tilde{A}_d^{\mathbf{ml}} = -\left( (h_d A)^{\mathbf{ml}} \frac{v_d}{\sqrt{2}} + \mu \frac{v_u}{\sqrt{2}} h_d^{\mathbf{ml}} \right). \quad (\text{A.2})$$

We include  $\tilde{A}$  and  $\tilde{A}_d$  in the mass insertion approximation, and separately diagonalise the  $3 \times 3$  slepton ( or down squark) doublet and singlet mass matrices. Bold face indices indicate these slepton or squark mass eigenstate bases, see Appendix C for details. Lepton and down quark mass eigenstate indices are in ordinary type.

We also define

$$I(m_1, m_2) = -\frac{1}{16\pi^2} \frac{m_1^2}{m_1^2 - m_2^2} \ln \frac{m_1^2}{m_2^2}, \quad (\text{A.3})$$

$$\begin{aligned} I(m_1, m_2, m_3) &= \int \frac{d^4 k}{(2\pi)^4} \frac{1}{k^2 + m_1^2} \frac{1}{k^2 + m_2^2} \frac{1}{k^2 + m_3^2} \\ &= \frac{1}{m_1^2 - m_2^2} \left( I(m_1, m_3) - I(m_2, m_3) \right), \end{aligned} \quad (\text{A.4})$$

$$\begin{aligned} I(m_1, m_2, m_3, m_4) &= \frac{1}{m_1^2 - m_2^2} \left[ \frac{1}{m_1^2 - m_3^2} \left( I(m_1, m_4) \right. \right. \\ &\quad \left. \left. - I(m_3, m_4) \right) - \frac{1}{m_2^2 - m_3^2} \left( I(m_2, m_4) - I(m_3, m_4) \right) \right], \end{aligned} \quad (\text{A.5})$$

$$\begin{aligned} I(m_1, m_2, m_3, m_4, m_5) &= \\ &= \frac{1}{m_1^2 - m_2^2} \left[ \left( I(m_1, m_3, m_4, m_5) - I(m_2, m_3, m_4, m_5) \right) \right]. \end{aligned} \quad (\text{A.6})$$

- Diagram 1.  $R_p$ -violation at II and VII from  $\lambda$  couplings.

$$(II, VII) = - \sum_{l, \mathbf{k}, \mathbf{m}} \lambda^{ilk} \lambda^{jml} m_{e_l} \tilde{A}^{\mathbf{mk}} I(m_{e_l}, m_{\tilde{E}_{\mathbf{k}}}, m_{\tilde{L}_{\mathbf{m}}}) + (i \leftrightarrow j) \quad (\text{A.7})$$

which can be rewritten as

$$(II, VII) = \sum_{l, k} \lambda^{ilk} \lambda^{jkl} m_{e_l} m_{e_k} (A + \mu_4 \tan \beta) I(m_{e_l}, m_{\tilde{E}_k}, m_{\tilde{L}_k}) + (i \leftrightarrow j) \quad (\text{A.8})$$

when we take  $\tilde{A}^{\mathbf{mk}}$  to be diagonal.

- Diagram 2.  $R_p$ -violation at II and VII from  $\lambda'$  couplings.

$$(II, VII) = -3 \sum_{l, \mathbf{k}, \mathbf{m}} \lambda'^{ilk} \lambda'^{jml} m_{d_l} \tilde{A}_d^{\mathbf{mk}} I(m_{d_l}, m_{\tilde{D}_{\mathbf{k}}}, m_{\tilde{Q}_{\mathbf{m}}}) + (i \leftrightarrow j) \quad (\text{A.9})$$

which can be rewritten as

$$(II, VII) = 3 \sum_{l, k} \lambda'^{ilk} \lambda'^{jkl} m_{d_l} m_{d_k} (A + \mu_4 \tan \beta) I(m_{d_l}, m_{\tilde{D}_k}, m_{\tilde{Q}_k}) + (i \leftrightarrow j) \quad (\text{A.10})$$

when we take  $\tilde{A}_d^{\mathbf{mk}}$  to be diagonal.

- Diagram 3.  $R_p$ -violation at (IV, VI) in the Grossman-Haber diagram.

$$(IV, VI) = \sum_{\alpha, \mathbf{k}, \mathbf{m}} \frac{g^{ik} B^i g^{j\mathbf{m}} B^j}{4 \cos^2 \beta} (Z_{\alpha 2}^* - Z_{\alpha 1}^* g'/g)^2 m_{\chi_\alpha^0} \left\{ I(m_h, m_{\tilde{\nu}_{\mathbf{k}}}, m_{\tilde{\nu}_{\mathbf{m}}}, m_{\chi_\alpha^0}) \cos^2(\alpha - \beta) \right. \\ \left. + I(m_H, m_{\tilde{\nu}_{\mathbf{k}}}, m_{\tilde{\nu}_{\mathbf{m}}}, m_{\chi_\alpha^0}) \sin^2(\alpha - \beta) - I(m_A, m_{\tilde{\nu}_{\mathbf{k}}}, m_{\tilde{\nu}_{\mathbf{m}}}, m_{\chi_\alpha^0}) \right\} \quad (\text{A.11})$$

- Diagram 4.  $R_p$ -violation at (I, VII) and (II, VIII) from  $\lambda' - \lambda'$  diagram.

$$(I, VII) + (II, VIII) = 3 \sum_{\alpha, l, \mathbf{k}, \mathbf{m}} \mu_i \frac{Z_{\alpha 3}^* Z_{\alpha 4}^*}{m_{\chi_\alpha}} h_d^{kl} m_{d_k} \lambda'^{j\mathbf{m}k} \tilde{A}_d^{\mathbf{ml}} I(m_{d_k}, m_{\tilde{D}_1}, m_{\tilde{Q}_{\mathbf{m}}}) \\ + 3 \sum_{\alpha, l, \mathbf{k}, \mathbf{m}} \mu_j \frac{Z_{\alpha 3}^* Z_{\alpha 4}^*}{m_{\chi_\alpha}} h_d^{kl} m_{d_k} \lambda'^{i\mathbf{m}k} \tilde{A}_d^{\mathbf{ml}} \\ I(m_{d_k}, m_{\tilde{D}_1}, m_{\tilde{Q}_{\mathbf{m}}}) \quad (\text{A.12})$$

which simplifies to

$$(I, VII) + (II, VIII) = -3 \sum_{\alpha, k} \mu_j \frac{Z_{\alpha 3}^* Z_{\alpha 4}^*}{m_{\chi_\alpha}} h_d^{kl} m_{d_k}^2 \lambda'^{ikk} (A + \mu_4 \tan \beta) \\ I(m_{d_k}, m_{\tilde{D}_k}, m_{\tilde{Q}_k}) + (i \leftrightarrow j) \quad (\text{A.13})$$

when both  $h_d^{kl}$  and  $\tilde{A}_d^{\mathbf{ml}}$  are taken to be diagonal.

- Diagram 5  $R_p$ -violation at II and VI from  $\lambda - \lambda$  diagram.

$$(II, VI) = \sum_{\mathbf{l}, \mathbf{m}} \lambda^{ijl} m_{e_j} h_e^{jj} \tilde{A}^{\mathbf{ml}} B_{\mathbf{m}} \tan \beta I(m_{e_j}, m_{\tilde{E}_1}, m_{\tilde{L}_{\mathbf{m}}}, m_{H^+}) + (i \leftrightarrow j) \quad (\text{A.14})$$

which reduces to

$$(II, VI) = - \sum_l \lambda^{ijl} m_{e_j} m_{e_l} h_e^j (A + \mu_4 \tan \beta) B_l \tan \beta I(m_{e_j}, m_{\tilde{E}_1}, m_{\tilde{L}_l}, m_{H^+}) + (i \leftrightarrow j) \quad (\text{A.15})$$

when we take  $\tilde{A}^{\mathbf{ml}}$  diagonal.

- Diagram 6.  $R_p$ -violation at (I,VII) and (II,VIII) from  $\lambda - \lambda$  diagram.

$$\begin{aligned} (I, VII) + (II, VIII) &= \sum_{\alpha, \mathbf{l}, k, \mathbf{m}} \mu_i \frac{Z_{\alpha 3}^* Z_{\alpha 4}^*}{m_{\chi_\alpha}} h_e^{k1} m_{e_k} \lambda^{j\mathbf{m}k} \tilde{A}^{\mathbf{ml}} I(m_{e_k}, m_{\tilde{E}_1}, m_{\tilde{L}_{\mathbf{m}}}) \\ &+ \sum_{\alpha, \mathbf{l}, k, \mathbf{m}} \mu_j \frac{Z_{\alpha 3}^* Z_{\alpha 4}^*}{m_{\chi_\alpha}} h_e^{k1} m_{e_k} \lambda^{i\mathbf{m}k} \tilde{A}^{\mathbf{ml}} \\ &I(m_{e_k}, m_{\tilde{E}_1}, m_{\tilde{L}_{\mathbf{m}}}) \end{aligned} \quad (\text{A.16})$$

which simplifies to

$$\begin{aligned} (I, VII) + (II, VIII) &= - \sum_{\alpha, k} \mu_j \frac{Z_{\alpha 3}^* Z_{\alpha 4}^*}{m_{\chi_\alpha}} h_e^k m_{e_k}^2 \lambda^{ikk} (A + \mu_4 \tan \beta) \\ &I(m_{e_k}, m_{\tilde{E}_k}, m_{\tilde{L}_k}) + (i \leftrightarrow j) \end{aligned} \quad (\text{A.17})$$

when both  $h_e^{k1}$  and  $\tilde{A}^{\mathbf{ml}}$  are taken to be diagonal.

- Diagram 7.  $R_p$ -violation at I and V from  $\lambda - \lambda$  diagram.

$$(I, V) = \sum_{\alpha, \mathbf{l}, k} \mu_i \frac{Z_{\alpha 3}^* Z_{\alpha 4}^*}{m_{\chi_\alpha}} h_e^{j1} (h_e^{k1} \mu_k \frac{v_u}{\sqrt{2}} \sin^2 \beta) h_e^{jj} m_e^j I(m_{e_j}, m_{\tilde{E}_1}, m_{H^+}) + (i \leftrightarrow j). \quad (\text{A.18})$$

Taking the lepton Yukawa couplings to be diagonal this simplifies to

$$(I, V) = \sum_{\alpha} \mu_i \frac{Z_{\alpha 3}^* Z_{\alpha 4}^*}{m_{\chi_\alpha}} (h_e^j)^2 (h_e^j \mu_j \frac{v_u}{\sqrt{2}} \sin^2 \beta) m_e^j I(m_{e_j}, m_{\tilde{E}_j}, m_{H^+}) + (i \leftrightarrow j). \quad (\text{A.19})$$

- Diagram 8.  $R_p$ -violation at II and V from  $\lambda - \lambda$  diagram.

$$(II, V) = - \sum_{\mathbf{k}, m} \lambda^{ijk} m_{e_j} h_e^{jj} \mu_m h_e^{mk} \frac{v_u}{\sqrt{2}} \sin^2 \beta I(m_{e_j}, m_{\tilde{E}_k}, m_{H^+}) + (i \leftrightarrow j). \quad (\text{A.20})$$

which becomes

$$(II, V) = - \sum_k \lambda^{ijk} m_{e_j} h_e^{jj} \mu_k h_e^k \frac{v_u}{\sqrt{2}} \sin^2 \beta I(m_{e_j}, m_{\tilde{E}_k}, m_{H^+}) + (i \leftrightarrow j). \quad (\text{A.21})$$

for diagonal Yukawa couplings.

- Diagram 9.  $R_p$ -violation at III and V from  $\lambda - \lambda$  diagram.

$$(III, V) = \sum_{\alpha, \mathbf{k}, n} \frac{v_u}{\sqrt{2}} \sin^2 \beta \mu_n \mu_j m_{e_j} h_e^{jj} h_e^{ik} h_e^{nk} V_{\alpha 2}^* U_{\alpha 2}^* m_{\chi_\alpha}^+ I(m_{e_j}, m_{\tilde{E}_k}, m_{H^+}, m_{\chi_\alpha}^+) + (i \leftrightarrow j) \quad (\text{A.22})$$

which simplifies to

$$(III, V) = \sum_\alpha \frac{v_u}{\sqrt{2}} \sin^2 \beta \mu_i \mu_j m_{e_j} h_e^j h_e^{i2} V_{\alpha 2}^* U_{\alpha 2}^* m_{\chi_\alpha}^+ I(m_{e_j}, m_{\tilde{E}_i}, m_{H^+}, m_{\chi_\alpha}^+) + (i \leftrightarrow j) \quad (\text{A.23})$$

for diagonal Yukawa couplings.

- Diagram 10.  $R_p$ -violation at III and VIII from  $\lambda - \lambda$  diagram.

$$(III, VIII) = - \sum_{\alpha, \beta, \mathbf{k}, \mathbf{l}, m} h_e^{ik} \tilde{A}^{\mathbf{l}\mathbf{k}} h_e^{\mathbf{l}m} m_{e_m} \mu_m \mu_j m_{\chi_\alpha}^+ V_{\alpha 2}^* U_{\alpha 2}^* \times \frac{Z_{\beta 3}^* Z_{\beta 4}^*}{m_{\chi_\beta}^o} I(m_{e_m}, m_{\tilde{E}_k}, m_{\tilde{L}_1}, m_{\chi_\alpha}^+) + (i \leftrightarrow j) \quad (\text{A.24})$$

when we take diagonal Yukawa couplings this reduces to

$$(III, VIII) = \sum_{\alpha, \beta, m} (A + \mu_4 \tan \beta) h_e^{i2} m_e^{i2} \mu_i \mu_j m_{\chi_\alpha}^+ V_{\alpha 2}^* U_{\alpha 2}^* \times \frac{Z_{\beta 3}^* Z_{\beta 4}^*}{m_{\chi_\beta}^o} I(m_{e_i}, m_{\tilde{E}_i}, m_{\tilde{L}_i}, m_{\chi_\alpha}^+) + (i \leftrightarrow j) \quad (\text{A.25})$$

- Diagram 11.  $R_p$ -violation at I and VI from  $\lambda - \lambda$  diagram.

$$(I, VI) = - \sum_{\alpha, \mathbf{l}, \mathbf{m}} \mu_i \frac{Z_{\alpha 3}^* Z_{\alpha 4}^*}{m_{\chi_\alpha^0}} h_e^{j\mathbf{l}} h_e^{j\mathbf{j}} m_{e_j} \tilde{A}^{\mathbf{ml}} B_{\mathbf{m}} \tan \beta I(m_{e_j}, m_{\tilde{E}_1}, m_{\tilde{L}_m}, m_{H^-}) + (i \leftrightarrow j) \quad (\text{A.26})$$

This reduces to

$$(I, VI) = \sum_{\alpha} \mu_i \frac{Z_{\alpha 3}^* Z_{\alpha 4}^*}{m_{\chi_\alpha^0}} (h_e^{jj} m_{e_j})^2 (A + \mu_4 \tan \beta) B_j \tan \beta I(m_{e_j}, m_{\tilde{E}_j}, m_{\tilde{L}_j}, m_{H^-}) + (i \leftrightarrow j) \quad (\text{A.27})$$

with diagonal Yukawa couplings.

- Diagram 12.  $R_p$ -violation at III and VII from  $\lambda - \lambda$  diagram.

$$(III, VII) = \sum_{\alpha, \mathbf{k}, \mathbf{l}, \mathbf{m}} h_e^{i\mathbf{k}} \tilde{A}^{\mathbf{lk}} \lambda^{j\mathbf{l}\mathbf{m}} m_{e_m} \mu_m V_{\alpha 2}^* U_{\alpha 2}^* m_{\chi_\alpha^+} I(m_{e_m}, m_{\tilde{E}_k}, m_{\tilde{L}_1}, m_{\chi_\alpha^+}) + (i \leftrightarrow j) \quad (\text{A.28})$$

With diagonal Yukawa couplings this reduces to

$$(III, VII) = - \sum_{\alpha, \mathbf{m}} h_e^{ii} m_{e_i} (A + \mu_4 \tan \beta) \lambda_{j\mathbf{i}\mathbf{m}} m_{e_m} \mu_m V_{\alpha 2}^* U_{\alpha 2}^* m_{\chi_\alpha^+} I(m_{e_m}, m_{\tilde{E}_i}, m_{\tilde{L}_i}, m_{\chi_\alpha^+}) + (i \leftrightarrow j). \quad (\text{A.29})$$

- Diagram 13.  $R_p$ -violation at III and VI from  $\lambda - \lambda$  diagram.

$$(III, VI) = - \sum_{\alpha, \mathbf{k}, \mathbf{l}} h_e^{i\mathbf{k}} \tilde{A}^{\mathbf{lk}} B_1 \tan \beta h_e^{jj} m_{e_j} \mu_j V_{\alpha 2}^* U_{\alpha 2}^* m_{\chi_\alpha^+} I(m_{e_j}, m_{\tilde{E}_k}, m_{\tilde{L}_1}, m_{H^+}, m_{\chi_\alpha^+}) + (i \leftrightarrow j) \quad (\text{A.30})$$

which reduces to

$$(III, VI) = \sum_{\alpha} (A + \mu_4 \tan \beta) h_e^i m_{e_i} h_e^j m_{e_j} B_i \mu_j V_{\alpha 2}^* U_{\alpha 2}^* m_{\chi_\alpha^+} I(m_{e_j}, m_{\tilde{E}_i}, m_{\tilde{L}_i}, m_{H^+}, m_{\chi_\alpha^+}) + (i \leftrightarrow j). \quad (\text{A.31})$$

- Diagram 14.  $R_p$ -violation at III and IV in  $g - \lambda$  loop.

$$(III, IV) = - \sum_{\alpha, l} \frac{g^{il}}{\sqrt{2}} U_{\alpha 1}^* V_{\alpha 2}^* m_{\chi_\alpha}^+ \mu_j m_{e_j} h_e^{jj} B_1 \tan \beta I(m_{e_j}, m_{\tilde{L}_1}, m_{H^+}, m_{\chi_\alpha^+}) + (i \leftrightarrow j) \quad (A.32)$$

which reduces for  $g^{i1} = g$  to

$$(III, IV) = - \sum_{\alpha} \frac{g}{\sqrt{2}} U_{\alpha 1}^* V_{\alpha 2}^* m_{\chi_\alpha}^+ \mu_j m_{e_j} h_e^{jj} B_i \tan \beta I(m_{e_j}, m_{\tilde{L}_i}, m_{H^+}, m_{\chi_\alpha^+}) + (i \leftrightarrow j) \quad (A.33)$$

- Diagram 15.  $R_p$ -violation at III and VIII in  $g - \lambda$  loop.

$$(III, VIII) = - \sum_{\alpha, \beta, k, l} \frac{g^{il}}{\sqrt{2}} h_e^{lk} m_{e_k} \mu_k \mu_j V_{\alpha 2}^* U_{\alpha 1}^* m_{\chi_\alpha}^+ \frac{Z_{\beta 3}^* Z_{\beta 4}^*}{m_{\chi_\beta}^o} I(m_{e_k}, m_{\tilde{L}_1}, m_{\chi_\alpha^+}) + (i \leftrightarrow j) \quad (A.34)$$

When the charged slepton mass eigenstates are aligned with the charged lepton mass eigenstates, this becomes

$$(III, VIII) = - \sum_{\alpha, \beta} \frac{g}{\sqrt{2}} h_e^i m_{e_i} \mu_i \mu_j V_{\alpha 2}^* U_{\alpha 1}^* m_{\chi_\alpha}^+ \frac{Z_{\beta 3}^* Z_{\beta 4}^*}{m_{\chi_\beta}^o} I(m_{e_i}, m_{\tilde{L}_i}, m_{\chi_\alpha^+}) + (i \leftrightarrow j) \quad (A.35)$$

- Diagram 16  $R_p$ -violation at I and III in  $g - \lambda$  loop.

There are two possible diagrams with  $\mathcal{R}_p$  at I and III. Firstly the neutralino can arrive as a  $\tilde{h}_d$  at vertex II, where a  $\tilde{w}^-$  is absorbed. Secondly the neutralino can arrive as a gaugino, in which case the  $\tilde{h}_d^-$  part of the chargino is absorbed.

$$(I, III) = - \sum_{\alpha, \beta} \frac{g}{\sqrt{2}} \sin^2 \beta h_e^{jj} m_{e_j} \mu_i \mu_j V_{\alpha 2}^* U_{\alpha 1}^* m_{\chi_\alpha}^+ \frac{Z_{\beta 3}^* Z_{\beta 4}^*}{m_{\chi_\beta}^o} I(m_{e_j}, m_{H^+}, m_{\chi_\alpha^+}) \\ - \sum_{\alpha, \beta} \frac{g}{\sqrt{2}} \sin^2 \beta h_e^{jj} m_{e_j} \mu_i \mu_j V_{\alpha 2}^* U_{\alpha 2}^* m_{\chi_\alpha}^+ \frac{(Z_{\beta 2}^* - Z_{\beta 1}^* g'/g) Z_{\beta 3}^*}{m_{\chi_\beta}^o} \times \\ I(m_{e_j}, m_{H^+}, m_{\chi_\alpha^+}) + (i \leftrightarrow j) \quad (A.36)$$

- Diagram 17  $R_p$ -violation at I and VII in  $g - \lambda$  loop. We also include here the  $g - \lambda'$  loop of similar form, with sleptons/leptons replaced by squarks and quarks. This loop is a scale-dependent correction to  $\delta_\mu^i$ , which changes the mass

and eigenvector of the neutrino who gets mass at tree-level. We fix  $Q^2 = m_{\tilde{L}_3}^2$  in  $B_0(p^2 = 0, m_1, m_2) = I(m_1, m_2) - \ln(m_2^2/Q^2) + 1$ .

$\tilde{W}^o - \nu$  mixing gives:

$$(I, VII) = \sum_{\alpha, k, 1} \frac{g^{k1}}{\sqrt{2}} m_{e_k} \mu_i \frac{Z_{\alpha 3}^* Z_{\alpha 2}^*}{m_{\chi_\alpha^o}} \lambda^{1jk} B_0(0, m_{e_k}, m_{\tilde{L}_1}) + 3 \sum_{\alpha, k, 1} \frac{g^{k1}}{\sqrt{2}} m_{d_k} \mu_i \frac{Z_{\alpha 3}^* Z_{\alpha 2}^*}{m_{\chi_\alpha^o}} \lambda'^{j1k} B_0(0, m_{d_k}, m_{\tilde{Q}_1}) + (i \leftrightarrow j) \quad (A.37)$$

and  $\tilde{B} - \nu$  mixing gives

$$(I, VII) = - \sum_{\alpha, k, 1} m_{e_k} \mu_i \frac{Z_{\alpha 3}^* Z_{\alpha 1}^*}{m_{\chi_\alpha^o}} \left\{ \frac{g'^{k1}}{\sqrt{2}} \lambda^{1jk} B_0(0, m_{e_k}, m_{\tilde{L}_1}) - 2 \frac{g'^{k1}}{\sqrt{2}} \lambda^{kj1} B_0(0, m_{e_k}, m_{\tilde{E}_1}) \right\} - \sum_{\alpha, k, 1} m_{d_k} \mu_i \frac{Z_{\alpha 3}^* Z_{\alpha 1}^*}{m_{\chi_\alpha^o}} \left\{ \frac{g'^{k1}}{\sqrt{2}} \lambda'^{j1k} B_0(0, m_{d_k}, m_{\tilde{Q}_1}) - 2 \frac{g'^{k1}}{\sqrt{2}} \lambda'^{jk1} B_0(0, m_{d_k}, m_{\tilde{D}_1}) \right\} + (i \leftrightarrow j) \quad (A.38)$$

(Notice that the  $g'^{k1}$  appearing in different terms have absorbed different rotation matrices, so are not the same. See equation (B.30) for formulae with explicit diagonalisation matrices.)

We can set  $g^{k1} = g$ ,  $g'^{k1} = g'$  and  $k = 1$  in the above expression if the sfermion and fermion mass eigenstate bases are the same.

- Diagram 18  $R_p$ -violation at III and VII in  $g - \lambda$  loop; as noted in ref. [12], this is zero if the sleptons are mass-degenerate.

$$(III, VII) = \sum_{\alpha, k, 1} \frac{g^{i1}}{\sqrt{2}} m_{e_k} \mu_k V_{\alpha 2}^* U_{\alpha 1}^* m_{\chi_\alpha^+} \lambda^{1jk} I(m_{e_k}, m_{\tilde{L}_1}, m_{\chi_\alpha^+}) + (i \leftrightarrow j) \quad (A.39)$$

which reduces for  $g^{k1} = g$  to

$$(III, VII) = \sum_{\alpha, k} \frac{g}{\sqrt{2}} m_{e_k} \mu_k V_{\alpha 2}^* U_{\alpha 1}^* m_{\chi_\alpha^+} \lambda^{ijk} I(m_{e_k}, m_{\tilde{L}_1}, m_{\chi_\alpha^+}) + (i \leftrightarrow j) \quad (A.40)$$

- Diagram 19  $R_p$ -violation at I and VI in Grossman-Haber loop.

We neglected this diagram in our previous paper—the expression for the amplitude is lengthy. In the interaction eigenstate basis, the incident neutrino can turn into an up-type higgsino/down-type higgsino (gaugino), which subsequently turns into a gaugino and up/down Higgs (an up- or down-type Higgs and higgsino) at the vertex II. In mass eigenstate basis, these possibilities generate a number of terms:

$$\begin{aligned}
(I, VI) + (IV, VIII) = & \sum_{\alpha, \beta, 1} \frac{gg^{j1}}{4 \cos \beta} \mu_i \frac{Z_{\alpha 3}^*}{m_{\chi_\alpha^0}} m_{\chi_\beta^0} (Z_{\beta 2}^* - Z_{\beta 1}^* g'/g) B_1 \times \\
& \left\{ \left[ Z_{\alpha 3}^* (Z_{\beta 2}^* + Z_{\beta 1}^* g'/g) \cos \alpha - Z_{\alpha 4}^* (Z_{\beta 2}^* - Z_{\beta 1}^* g'/g) \sin \alpha + \right. \right. \\
& \quad \left. \left. (Z_{\alpha 2}^* + Z_{\beta 1}^* g'/g) Z_{\beta 3}^* \cos \alpha - (Z_{\alpha 2}^* - Z_{\alpha 1}^* g'/g) Z_{\beta 4}^* \sin \alpha \right] \times \right. \\
& \quad \left. \cos(\alpha - \beta) I(m_h, m_{\chi_\beta^0}, m_{\tilde{\nu}_1}) \right. \\
& + \left[ Z_{\alpha 3}^* (Z_{\beta 2}^* + Z_{\beta 1}^* g'/g) \sin \alpha + Z_{\alpha 4}^* (Z_{\beta 2}^* - Z_{\beta 1}^* g'/g) \cos \alpha \right. \\
& \quad \left. + (Z_{\alpha 2}^* + Z_{\beta 1}^* g'/g) Z_{\beta 3}^* \sin \alpha + (Z_{\alpha 2}^* - Z_{\alpha 1}^* g'/g) Z_{\beta 4}^* \cos \alpha \right] \times \\
& \quad \left. \sin(\alpha - \beta) I(m_H, m_{\chi_\beta^0}, m_{\tilde{\nu}_1}) \right. \\
& + \left[ Z_{\alpha 3}^* (Z_{\beta 2}^* + Z_{\beta 1}^* g'/g) \cos \beta - Z_{\alpha 4}^* (Z_{\beta 2}^* - Z_{\beta 1}^* g'/g) \sin \beta + \right. \\
& \quad \left. (Z_{\alpha 2}^* + Z_{\beta 1}^* g'/g) Z_{\beta 3}^* \cos \beta - (Z_{\alpha 2}^* - Z_{\alpha 1}^* g'/g) Z_{\beta 4}^* \sin \beta \right] \times \\
& \quad \left. I(m_A, m_{\chi_\beta^0}, m_{\tilde{\nu}_1}) \right\} + (i \leftrightarrow j) \tag{A.41}
\end{aligned}$$

- Diagram 20  $\mathcal{R}_p$  at I and V with  $g - \lambda$  couplings. This differs from figure 2d): the internal line is a higgsino and there is an  $\tilde{A}$  mass insertion on the scalar line.

$$\begin{aligned}
(I, V) = & - \sum_{\alpha, \beta, \mathbf{m}} \mu_i \frac{g}{\sqrt{2}} \frac{Z_{\alpha 3}^*}{m_{\chi_\alpha^0}} \left\{ (Z_{\alpha 2}^* + Z_{\alpha 1}^* g'/g) U_{\beta 2}^* V_{\beta 2}^* + Z_{\alpha 3}^* U_{\beta 2}^* V_{\beta 1}^* \right\} m_{\chi_\beta^+} \\
& m_{e_{\mathbf{m}}} h_e^{j\mathbf{m}} \mu_{\mathbf{m}} \sin^2 \beta \tan \beta I(m_{\chi_\beta^+}, m_{\tilde{E}_{\mathbf{m}}}, m_{H^+}) + (i \leftrightarrow j) \tag{A.42}
\end{aligned}$$

which reduces for diagonal yukawas to

$$\begin{aligned}
(I, V) = & - \sum_{\alpha, \beta} \mu_i \frac{g}{\sqrt{2}} \frac{Z_{\alpha 3}^*}{m_{\chi_\alpha^0}} \left\{ (Z_{\alpha 2}^* + Z_{\alpha 1}^* g'/g) U_{\beta 2}^* V_{\beta 2}^* + Z_{\alpha 3}^* U_{\beta 2}^* V_{\beta 1}^* \right\} m_{\chi_\beta^+} \\
& m_{e_j} h_e^j \mu_j \sin^2 \beta \tan \beta \times I(m_{\chi_\beta^+}, m_{\tilde{E}_j}, m_{H^+}) + (i \leftrightarrow j) \tag{A.43}
\end{aligned}$$

- Diagram 21  $\mathcal{R}_p$  at I and IV with  $g - \lambda$  couplings.

The particle identities do not correspond to the labels on figure 2 d). The  $\nu_i$  can mix with a higgsino, then the loop fermion is a chargino, arriving at VII as  $\tilde{h}_d$ . Alternatively, the  $\nu_i$  turns into a gaugino, then there are two possibilities. Firstly, the loop fermion can be a higgsino, arriving at II as  $\tilde{h}_u$  and at VII as  $\tilde{h}_d$ . Secondly the loop fermion can be a charged lepton, and the scalar arriving at VII is a charged Higgs.

$$\begin{aligned}
(I, IV) = & \sum_{\beta, \alpha, \mathbf{p}, \mathbf{m}} \mu_i \frac{g}{\sqrt{2}} \frac{Z_{\alpha 3}^*}{m_{\chi_\alpha^0}} \left\{ (Z_{\alpha 2}^* + Z_{\alpha 1}^* g' / g) U_{\beta 2}^* V_{\beta 2}^* + Z_{\alpha 3}^* U_{\beta 2}^* V_{\beta 1}^* \right\} m_{\chi_\beta^+} \\
& h_e^{j\mathbf{m}} \tilde{A}^{\mathbf{p}\mathbf{m}} B_{\mathbf{p}} \tan \beta I(m_{\chi_\beta^+}, m_{\tilde{E}_{\mathbf{m}}}, m_{\tilde{L}_{\mathbf{p}}}, m_{H^+}) + (i \leftrightarrow j) \\
& - \sum_{\alpha, 1} \mu_i \frac{g^{j1}}{\sqrt{2}} \frac{Z_{\alpha 3}^* (Z_{\alpha 2}^* - Z_{\alpha 1}^* g' / g)}{m_{\chi_\alpha^0}} m_{e_j} h_e^{jj} \tan \beta B_1 \times \\
& I(m_{e_j}, m_{\tilde{L}_1}, m_{H^+}) + (i \leftrightarrow j)
\end{aligned} \tag{A.44}$$

which for diagonal yukawas reduces to

$$\begin{aligned}
(I, IV) = & - \sum_{\alpha, \beta} \mu_i \frac{g}{\sqrt{2}} \frac{Z_{\alpha 3}^*}{m_{\chi_\alpha^0}} \left\{ (Z_{\alpha 2}^* + Z_{\alpha 1}^* g' / g) U_{\beta 2}^* V_{\beta 2}^* + Z_{\alpha 3}^* U_{\beta 2}^* V_{\beta 1}^* \right\} m_{\chi_\beta^+} \times \\
& h_e^j m_{e_j} (A + \mu_4 \tan \beta) B_j \tan \beta I(m_{\chi_\beta^+}, m_{\tilde{E}_j}, m_{\tilde{L}_j}, m_{H^+}) + (i \leftrightarrow j) \\
& - \sum_{\alpha} \mu_i \frac{g}{\sqrt{2}} \frac{Z_{\alpha 3}^* (Z_{\alpha 2}^* - Z_{\alpha 1}^* g' / g)}{m_{\chi_\alpha^0}} m_{e_j} h_e^{jj} \tan \beta B_j \times \\
& I(m_{e_j}, m_{\tilde{L}_j}, m_{H^+}) + (i \leftrightarrow j)
\end{aligned} \tag{A.45}$$

## B. Basis-independent diagram amplitudes

In this appendix we write the contributions to the neutrino mass matrix  $[m_\nu]_{ij}$  from each diagram in terms of MSSM parameters and invariants. The latter can be evaluated in any basis.

We list all imaginable diagrams, and explain why some are zero or negligible. We write the MSSM parameters in the mass eigenstate basis, with diagonal quark and charged lepton mass matrices. See Appendix C for definitions of the matrices  $Z, U, V, L, E, Q$  and  $D$  which respectively diagonalise neutralinos, negative charginos, positive charginos, doublet charged sleptons, singlet sleptons, down-type doublet quarks and singlet down quarks.

We define

$$\tilde{A}^{ml} = -\hat{L}_M^m \left( (\lambda A)^{IMl} \frac{v_I}{\sqrt{2}} + \mu_I \frac{v_u}{\sqrt{2}} \lambda^{IMl} \right), \tag{B.1}$$

with  $\hat{L}^m = \lambda^m \cdot \vec{v}/|\lambda^m \cdot \vec{v}|$ , see equation (2.1). Similarly we define

$$\tilde{A}_d^{ml} = -\left((\lambda' A)^{Iml} \frac{v_I}{\sqrt{2}} + \mu_I \frac{v_u}{\sqrt{2}} \lambda'^{Iml}\right). \quad (\text{B.2})$$

Notice that the indices on  $\tilde{A}$  and  $\tilde{A}_d$  are in the charged lepton and down quark mass eigenstate basis respectively.

### B.1 $\lambda - \lambda$ diagrams—figure 2a)

- $R_p$ -violation at (I,VIII): this is a loop correction to the tree mass, so can be neglected.
- $R_p$ -violation at (I,VII) and (II,VIII) (diagram 6, equation A.16).

$$(I, VII) + (II, VIII) = \sum_{\alpha, l, k, m, p, n, q} \delta_\mu^i \delta_\lambda^{qn} m_{e^n} h_e^n |\mu| \tilde{A}^{kp} E_{nl} E_{pl}^* L_{qm} L_{km}^* \frac{Z_{\alpha 3}^* Z_{\alpha 4}^*}{m_{\chi_\alpha^0}} I(m_{e_n}, m_{\tilde{E}_l}, m_{\tilde{L}_m}) + (i \leftrightarrow j), \quad (\text{B.3})$$

which simplifies to

$$(I, VII) + (II, VIII) = -\sum_{\alpha, k} \delta_\mu^j \delta_\lambda^{kik} |\mu| h_e^k m_{e_k}^2 (A + |\mu| \tan \beta) \frac{Z_{\alpha 3}^* Z_{\alpha 4}^*}{m_{\chi_\alpha^0}} I(m_{e_k}, m_{\tilde{E}_k}, m_{\tilde{L}_k}) + (i \leftrightarrow j), \quad (\text{B.4})$$

when  $\tilde{A}, L$  and  $E$  are taken to be diagonal.

- $R_p$ -violation at (I, VI) (diagram 11, equation A.26)

$$(I, VI) = -\sum_{\alpha, l, p, r, q} \delta_\mu^i \delta_B^m (h_e^j)^2 m_{e_j} \tilde{A}^{qp} |B| |\mu| E_{jl} E_{pl}^* L_{mr} L_{qr}^* \tan \beta \frac{Z_{\alpha 3}^* Z_{\alpha 4}^*}{m_{\chi_\alpha^0}} I(m_{e_j}, m_{\tilde{E}_l}, m_{\tilde{L}_r}, m_{H^-}) + (i \leftrightarrow j), \quad (\text{B.5})$$

for diagonal  $\tilde{A}, L, E$  this simplifies to

$$(I, VI) = \sum_\alpha \delta_\mu^i \delta_B^j (h_e^j m_{e_j})^2 (A + |\mu| \tan \beta) |B| |\mu| \tan \beta \frac{Z_{\alpha 3}^* Z_{\alpha 4}^*}{m_{\chi_\beta^0}} I(m_{e_j}, m_{\tilde{E}_j}, m_{\tilde{L}_j}, m_{H^-}) + (i \leftrightarrow j). \quad (\text{B.6})$$

- $R_p$ -violation at (I,V) (diagram 7, equation A.18)

$$(I, V) = - \sum_{\alpha, l, k} \delta_\mu^i |\mu|^2 (h_e^j)^2 m_e^j m_e^k \delta_\mu^k \sin^2 \beta \tan \beta E_{jl} E_{kl}^* \frac{Z_{\alpha 3}^* Z_{\alpha 4}^*}{m_{\chi_\alpha}} I(m_{e_j}, m_{\tilde{E}_l}, m_{H^+}) + (i \leftrightarrow j). \quad (\text{B.7})$$

Taking  $\tilde{A}, L$  and  $E$  to be diagonal this simplifies to

$$(I, V) = - \sum_\alpha \delta_\mu^i \delta_\mu^j |\mu|^2 (m_e^j h_e^j)^2 \frac{Z_{\alpha 3}^* Z_{\alpha 4}^*}{m_{\chi_\alpha}} \sin^2 \beta \tan \beta I(m_{e_j}, m_{\tilde{E}_j}, m_{H^+}) + (i \leftrightarrow j). \quad (\text{B.8})$$

- $R_p$ -violation at (I,IV). This is not possible, because there is no  $R_p$ -violating mass involving two  $E^c$ .
- $R_p$ -violation at (I,II). This is not possible;  $\mathcal{R}_p$  at II requires three incident leptons.
- $R_p$ -violation at (II, VIII). This is included with  $R_p$ -violation at (I, VII).
- $R_p$ -violation at (II, VII) from  $\lambda$  couplings (diagram 1 equation A.7)

$$(II, VII) = - \sum_{l, m, n, r, p, q, s} \delta_\lambda^{inm} \delta_\lambda^{rjn} m_{e_n} \tilde{A}^{sq} E_{mp} E_{pq}^* L_{sl}^* L_{rl} I(m_{e_n}, m_{\tilde{E}_p}, m_{\tilde{L}_l}) + (i \leftrightarrow j), \quad (\text{B.9})$$

which can be rewritten as

$$(II, VII) = \sum_{l, k} \delta_\lambda^{ilk} \delta_\lambda^{jkl} m_{e_l} m_{e_k} (A + |\mu| \tan \beta) I(m_{e_l}, m_{\tilde{E}_k}, m_{\tilde{L}_k}) + (i \leftrightarrow j), \quad (\text{B.10})$$

when we take  $\tilde{A}, L$  and  $E$  to be diagonal.

- $R_p$ -violation at (II, VI) (diagram 5, equation A.14)

$$(II, VI) = \sum_{m, n, s, p, q, r} \delta_\lambda^{ijn} \delta_B^r |B| m_{e_j} h_e^j \tilde{A}^{pq} \tan \beta E_{ns} E_{qs}^* L_{pm}^* L_{rm} I(m_{e_j}, m_{\tilde{E}_s}, m_{\tilde{L}_m}, m_{H^+}) + (i \leftrightarrow j), \quad (\text{B.11})$$

which reduces to

$$(II, VI) = - \sum_l \delta_\lambda^{ijl} \delta_B^l |B| m_{e_j} m_{e_l} h_e^j (A + |\mu| \tan \beta) \tan \beta I(m_{e_j}, m_{\tilde{E}_l}, m_{\tilde{L}_l}, m_{H^+}) + (i \leftrightarrow j), \quad (\text{B.12})$$

when we take  $\tilde{A}, L$  and  $E$  diagonal.

- $R_p$ -violation at (II, V) (diagram 8, equation A.20)

$$(II, V) = - \sum_{k,l,m} \delta_\lambda^{ijk} \delta_\mu^m |\mu| m_{e_j} h_e^j m_{e_m} \tan \beta \sin^2 \beta E_{kl} E_{ml}^* I(m_{e_j}, m_{\tilde{E}_l}, m_{H^+}) + (i \leftrightarrow j), \quad (\text{B.13})$$

which becomes

$$(II, V) = - \sum_k \delta_\lambda^{ijk} \delta_\mu^k |\mu| m_{e_j} h_e^j m_{e^k} \tan \beta \sin^2 \beta I(m_{e_j}, m_{\tilde{E}_k}, m_{H^+}) + (i \leftrightarrow j), \quad (\text{B.14})$$

for diagonal matrices.

- $R_p$ -violation at (II, IV) is not possible because there is no  $\mathbb{R}_p$  mass between two  $E^c$ .
- $R_p$ -violation at (II, III) is not possible;  $\mathbb{R}_p$  at II requires three incident leptons.
- $R_p$ -violation at (III, VIII) (diagram 10, equation A.24)

$$(III, VIII) = - \sum_{\alpha,\beta,k,l,m,q,p} \delta_\mu^m \delta_\mu^j |\mu|^2 h_e^i \tilde{A}^{pq} h_e^m m_{e_m} E_{ik} E_{qk}^* L_{pl}^* L_{ml} V_{\alpha 2}^* U_{\alpha 2}^* m_{\chi_\alpha^+} \frac{Z_{\beta 3}^* Z_{\beta 4}^*}{m_{\chi_\beta^0}} I(m_{e_m}, m_{\tilde{E}_k}, m_{\tilde{L}_l}, m_{\chi_\alpha^+}) + (i \leftrightarrow j), \quad (\text{B.15})$$

when we take diagonal  $\tilde{A}$ ,  $L$  and  $E$  this reduces to

$$(III, VIII) = \sum_{\alpha,\beta} \delta_\mu^i \delta_\mu^j |\mu|^2 (A + |\mu| \tan \beta) (h_e^i m_e^i)^2 V_{\alpha 2}^* U_{\alpha 2}^* m_{\chi_\alpha^+} \frac{Z_{\beta 3}^* Z_{\beta 4}^*}{m_{\chi_\beta^0}} I(m_{e_i}, m_{\tilde{E}_i}, m_{\tilde{L}_i}, m_{\chi_\alpha^+}) + (i \leftrightarrow j). \quad (\text{B.16})$$

- $R_p$ -violation at (III, VII) (diagram 12, equation A.28)

$$(III, VII) = \sum_{\alpha,k,l,m,n,q,p} \delta_\lambda^{jnm} \delta_\mu^m |\mu| h_e^i \tilde{A}^{qp} m_{e_m} V_{\alpha 2}^* U_{\alpha 2}^* m_{\chi_\alpha^+} L_{nl} L_{ql}^* E_{ik} E_{pk}^* I(m_{e_m}, m_{\tilde{E}_k}, m_{\tilde{L}_l}, m_{\chi_\alpha^+}) + (i \leftrightarrow j), \quad (\text{B.17})$$

which becomes, when  $\tilde{A}$ ,  $L$  and  $E$  are diagonal

$$(III, VII) = - \sum_{\alpha, m} \delta_\lambda^{jm} \delta_\mu^m |\mu| h_e^i m_{e_m} m_{e_i} (A + |\mu| \tan \beta) V_{\alpha 2}^* U_{\alpha 2}^* m_{\chi_\alpha^+} I(m_{e_m}, m_{\tilde{E}_i}, m_{\tilde{L}_i}, m_{\chi_\alpha^+}) + (i \leftrightarrow j). \quad (B.18)$$

- $R_p$ -violation at (III, VI) (diagram 13, equation A.30).

$$(III, VI) = - \sum_{\alpha, k, l, m, q, p} \delta_\mu^j \delta_B^m |\mu| |B| h_e^i \tilde{A}^{qp} \tan \beta h_e^j m_{e_j} V_{\alpha 2}^* U_{\alpha 2}^* m_{\chi_\alpha^+} E_{ik} E_{pk}^* L_{ql}^* L_{ml} I(m_{e_j}, m_{\tilde{E}_k}, m_{\tilde{L}_l}, m_{H^+}, m_{\chi_\alpha^+}) + (i \leftrightarrow j), \quad (B.19)$$

which reduces to

$$(III, VI) = \sum_{\alpha} \delta_\mu^j \delta_\mu^i |\mu| |B| (A + |\mu| \tan \beta) h_e^i m_{e_i} h_e^j m_{e_j} V_{\alpha 2}^* U_{\alpha 2}^* m_{\chi_\alpha^+} I(m_{e_j}, m_{\tilde{E}_i}, m_{\tilde{L}_i}, m_{H^+}, m_{\chi_\alpha^+}) + (i \leftrightarrow j), \quad (B.20)$$

for diagonal  $\tilde{A}$ ,  $L$  and  $E$ .

- $R_p$ -violation at (III, V) (diagram 9, equation A.22).

$$(III, V) = \sum_{\alpha, k, n} \delta_\mu^n \delta_\mu^j |\mu|^2 \tan \beta m_e^n \sin^2 \beta m_{e_j} h_e^j h_e^i E_{ik} E_{nk}^* V_{\alpha 2}^* U_{\alpha 2}^* m_{\chi_\alpha^+} I(m_{e_j}, m_{\tilde{E}_k}, m_{H^+}, m_{\chi_\alpha^+}) + (i \leftrightarrow j), \quad (B.21)$$

which simplifies to

$$(III, V) = \sum_{\alpha} \delta_\mu^i \delta_\mu^j |\mu|^2 \tan \beta \sin^2 \beta m_{e_i} m_{e_j} h_e^j h_e^i V_{\alpha 2}^* U_{\alpha 2}^* m_{\chi_\alpha^+} I(m_{e_j}, m_{\tilde{E}_i}, m_{H^+}, m_{\chi_\alpha^+}) + (i \leftrightarrow j), \quad (B.22)$$

for diagonal  $E$ .

- $R_p$ -violation at (III, IV), is not possible because there is no  $\mathbb{R}_p$  mass involving two  $E_c$ .
- $R_p$ -violation at (IV, VIII) is not possible, for the same reason as (III, IV)—No diagram with  $E^c$  leaving VII and arriving at V can have  $R_p$ -violation at IV, so no diagrams with  $\mathbb{R}_p$  at (IV, ...) are possible.

- $R_p$ -violation at (V, VIII) is the same as (I, V).
- $R_p$ -violation at (V, VII) is the same as (II, V).
- $R_p$ -violation at (V, VI) is not possible, because we cannot put two units of lepton number violation on one charged line.
- $R_p$ -violation at (VI, VIII) is not possible because  $H^+$  has no  $R_p$  conserving mass with  $E^c$ .
- $R_p$ -violation at (VI, VII) is not possible because  $H^+$  has no  $R_p$  conserving mass with  $E^c$ .

## B.2 $\lambda' - \lambda'$ diagrams—figure 2b)

- $R_p$ -violation at (I,VIII) is a loop correction to the tree mass.
- $R_p$ -violation at (I,VII) and (II,VIII) from  $\lambda'$  couplings (diagram 4, equation A.12).

$$\begin{aligned}
(I, VII) + (II, VIII) &= 3 \sum_{\alpha, l, k, m, q, p, r} \delta_\mu^i |\mu| \frac{Z_{\alpha 3}^* Z_{\alpha 4}^*}{m_{\chi_\alpha}} h_d^k m_{d_k} \delta_{\lambda'}^{jrk} D_{kl} D_{ql}^* Q_{pm}^* Q_{rm} \tilde{A}_d^{pq} \\
&\quad I(m_{d_k}, m_{\tilde{D}_l}, m_{\tilde{Q}_m}) \\
&+ 3 \sum_{\alpha, l, k, m, q, p, r} \delta_\mu^j |\mu| \frac{Z_{\alpha 3}^* Z_{\alpha 4}^*}{m_{\chi_\alpha}} h_d^k m_{d_k} \delta_{\lambda'}^{irk} D_{kl} D_{ql}^* Q_{pm}^* Q_{rm} \tilde{A}_d^{pq} \\
&\quad I(m_{d_k}, m_{\tilde{D}_l}, m_{\tilde{Q}_m}), \tag{B.23}
\end{aligned}$$

which simplifies to

$$\begin{aligned}
(I, VII) + (II, VIII) &= -3 \sum_{\alpha, k} \delta_\mu^j |\mu| \frac{Z_{\alpha 3}^* Z_{\alpha 4}^*}{m_{\chi_\alpha}} h_d^k m_{d_k}^2 \delta_{\lambda'}^{ikk} (A + |\mu| \tan \beta) \times \\
&\quad I(m_{d_k}, m_{\tilde{D}_k}, m_{\tilde{Q}_k}) + (i \leftrightarrow j), \tag{B.24}
\end{aligned}$$

when  $\tilde{A}_d, Q$  and  $D$  are taken to be diagonal.

- $R_p$ -violation at II and VII from  $\lambda'$  couplings (diagram 2, equation A.9).

$$\begin{aligned}
(II, VII) &= -3 \sum_{l, k, m, n, p, r, s} \delta_{\lambda'}^{ilp} \delta_{\lambda'}^{jnl} m_{d_l} \tilde{A}_d^{sr} D_{pk} D_{rk}^* L_{nm} L_{sm}^* \times \\
&\quad I(m_{d_l}, m_{\tilde{D}_k}, m_{\tilde{Q}_m}) + (i \leftrightarrow j), \tag{B.25}
\end{aligned}$$

which can be rewritten as

$$(II, VII) = 3 \sum_{l,k} \delta_{\chi'}^{ilk} \delta_{\chi'}^{jkl} m_{d_l} m_{d_k} (A + |\mu| \tan \beta) I(m_{d_l}, m_{\tilde{D}_k}, m_{\tilde{Q}_k}) + (i \leftrightarrow j), \quad (\text{B.26})$$

when we take  $\tilde{A}_d, Q$  and  $D$  to be diagonal.

- Lepton number violation is not possible inside a squark loop, so the only additional effect that bilinear  $\mathcal{R}_p$  can have is to induce squark flavour violation at V. We neglect this because the squark flavour violation is small:  $\delta_\mu^i \delta_{\chi'}^{ipq} |\mu| v_u$ . If we take  $m_\nu \lesssim \text{eV}$  then this implies  $\delta_\mu^i \lesssim 10^{-5}$ , so  $\delta_\mu^i \delta_{\chi'}^{ipq} |\mu| v_u \lesssim \delta_{\chi'}^{ipq} \text{GeV}^2$ , which is negligible. We differ here from reference [22], where this flavour violation due to the bilinears is included, but bilinear lepton number violation is not.

### B.3 the Grossman-Haber diagrams—figure 2c)

- $R_p$ -violation at (I, VIII) is a loop correction to the tree level mass, so negligible.
- $R_p$ -violation at (I, VI) and (IV, VIII) (diagram 19, equation A.41). The basis independent version of this diagram can be read off from equation (A.41), substituting  $\delta_B^n |B|$  for  $B^n$ , and  $\delta_\mu^i |\mu|$  for  $\mu^i$ .
- $R_p$ -violation at (IV, VI) (diagram 3, equation A.11)

$$(IV, VI) = \sum_{\alpha, l, m, k, n} \frac{g^2 \delta_B^m \delta_B^n |B|^2}{4 \cos^2 \beta} (Z_{\alpha 2}^* - Z_{\alpha 1}^* g'/g)^2 m_{\chi_\alpha^0} L_{il}^* L_{ml} L_{jk}^* L_{nk} \left\{ I(m_h, m_{\tilde{\nu}_l}, m_{\tilde{\nu}_k}, m_{\chi_\alpha^0}) \cos^2(\alpha - \beta) + I(m_H, m_{\tilde{\nu}_l}, m_{\tilde{\nu}_k}, m_{\chi_\alpha^0}) \sin^2(\alpha - \beta) - I(m_A, m_{\tilde{\nu}_l}, m_{\tilde{\nu}_k}, m_{\chi_\alpha^0}) \right\}, \quad (\text{B.27})$$

which for diagonal  $L$  becomes

$$(IV, VI) = \sum_\alpha \frac{g^2 \delta_B^i \delta_B^j |B|^2}{4 \cos^2 \beta} (Z_{\alpha 2}^* - Z_{\alpha 1}^* g'/g)^2 m_{\chi_\alpha^0} \left\{ I(m_h, m_{\tilde{\nu}_i}, m_{\tilde{\nu}_j}, m_{\chi_\alpha^0}) \cos^2(\alpha - \beta) + I(m_H, m_{\tilde{\nu}_i}, m_{\tilde{\nu}_j}, m_{\chi_\alpha^0}) \sin^2(\alpha - \beta) - I(m_A, m_{\tilde{\nu}_i}, m_{\tilde{\nu}_j}, m_{\chi_\alpha^0}) \right\}. \quad (\text{B.28})$$

### B.4 $g - \lambda$ diagrams—figure 2d)

- $R_p$ -violation at (I, VIII) would be a loop correction to the tree level mass, so is negligible.
- $R_p$ -violation at (I, VII) (diagram 17, equation A.37). See comments before equation A.37.

$\tilde{W}^0 - \nu$  mixing gives:

$$\begin{aligned}
(I, VII) &= \sum_{\alpha, k, l, m} \frac{g}{\sqrt{2}} m_{e_k} \delta_\mu^i |\mu| \delta_\lambda^{mjk} L_{kl}^* L_{ml} \frac{Z_{\alpha 3}^* Z_{\alpha 2}^*}{m_{\chi_\alpha^0}} B_0(0, m_{e_k}, m_{\tilde{L}_l}) \\
&+ 3 \sum_{\alpha, k, l, m} \frac{g}{\sqrt{2}} m_{d_k} \delta_\mu^i |\mu| \delta_{\lambda'}^{jmk} Q_{kl}^* Q_{ml} \frac{Z_{\alpha 3}^* Z_{\alpha 2}^*}{m_{\chi_\alpha^0}} B_0(0, m_{d_k}, m_{\tilde{Q}_l}) \\
&+ (i \leftrightarrow j)
\end{aligned} \tag{B.29}$$

and  $\tilde{B} - \nu$  mixing gives

$$\begin{aligned}
(I, VII) &= - \sum_{\alpha, k, l, m} \frac{g'}{\sqrt{2}} m_{e_k} \delta_\mu^i |\mu| \frac{Z_{\alpha 3}^* Z_{\alpha 1}^*}{m_{\chi_\alpha^0}} \left\{ \delta_\lambda^{mjk} L_{kl}^* L_{ml} B_0(0, m_{e_k}, m_{\tilde{L}_l}) \right. \\
&\quad \left. - 2 \delta_\lambda^{kjm} E_{kl}^* E_{ml} B_0(0, m_{e_k}, m_{\tilde{E}_l}) \right\} \\
&- \sum_{\alpha, k, l, m} \frac{g'}{\sqrt{2}} m_{d_k} \delta_\mu^i |\mu| \frac{Z_{\alpha 3}^* Z_{\alpha 1}^*}{m_{\chi_\alpha^0}} \left\{ \delta_{\lambda'}^{jmk} Q_{kl}^* Q_{ml} B_0(0, m_{d_k}, m_{\tilde{Q}_l}) \right. \\
&\quad \left. - 2 \delta_{\lambda'}^{jkm} D_{kl}^* D_{ml} B_0(0, m_{d_k}, m_{\tilde{D}_l}) \right\} + (i \leftrightarrow j)
\end{aligned} \tag{B.30}$$

The simplifications when  $E, L, Q$  and  $D$  are diagonal are obvious, so we do not repeat these expressions.

- $\mathcal{R}_p$  at (I,V) (diagram 20, equation A.42). The particle labels in figure 2d) do not apply in this case. The incident  $\nu_i$  mixes with a gaugino, and the internal fermion line is a higgsino, or  $\nu_i$  mixes with  $\tilde{h}_u$  and meets  $\tilde{w}^+$  at II. The scalar incident at VII is an  $E^c$ .

$$\begin{aligned}
(I, V) &= - \sum_{\alpha, \beta, l, m} \delta_\mu^i \delta_\mu^m |\mu|^2 \frac{g}{\sqrt{2}} \frac{Z_{\alpha 3}^*}{m_{\chi_\alpha^0}} \left\{ (Z_{\alpha 2}^* + Z_{\alpha 1}^* g'/g) U_{\beta 2}^* V_{\beta 2}^* + Z_{\alpha 3}^* U_{\beta 2}^* V_{\beta 1}^* \right\} \times \\
&\quad m_{\chi_\beta^+} m_{e_m} h_e^j \sin^2 \beta \tan \beta E_{jl} E_{ml}^* I(m_{\chi_\beta^+}, m_{\tilde{E}_l}, m_{H^+}) + (i \leftrightarrow j).
\end{aligned} \tag{B.31}$$

This reduces, when  $E$  is diagonal to

$$\begin{aligned}
(I, V) &= - \sum_{\alpha, \beta} \delta_\mu^i \delta_\mu^j |\mu|^2 \frac{g}{\sqrt{2}} \frac{Z_{\alpha 3}^*}{m_{\chi_\alpha^0}} \left\{ (Z_{\alpha 2}^* + Z_{\alpha 1}^* g'/g) U_{\beta 2}^* V_{\beta 2}^* + Z_{\alpha 3}^* U_{\beta 2}^* V_{\beta 1}^* \right\} m_{\chi_\beta^+} \\
&\quad m_{e_j} h_e^j \sin^2 \beta \tan \beta I(m_{\chi_\beta^+}, m_{\tilde{E}_j}, m_{H^+}) + (i \leftrightarrow j).
\end{aligned} \tag{B.32}$$

- $\mathcal{R}_p$  at (I,IV) (diagram 21, equation A.44). The neutrino can mix with a gaugino, then there are two possibilities, which we list separately. Firstly, the internal fermion line can be a higgsino. An  $\tilde{A}$  insertion on the scalar line ensures that

the incident scalar at VII is an  $E^c$ . The second possibility is for the gaugino to interact with  $\ell, \tilde{L}$  at II. In this case  $H^+$  and  $e^c$  are incident at VII. A third possibility is for the incident neutrino  $\nu_i$  could also mix with  $\tilde{h}_u$ , which meets a  $\tilde{w}$  at II, and emits a  $H_u^+$ . An  $\tilde{A}$  mass insertion on the scalar line, and  $m_{\chi^+}$  on the fermion line, ensure that  $E^c$  and  $\tilde{h}_d$  arrive at VII.

$$(I, IV)_1 = \sum_{\beta, \alpha, l, m, p, q, r} \delta_B^r \delta_\mu^i |\mu| |B| \frac{g}{\sqrt{2}} \frac{Z_{\alpha 3}^* (Z_{\alpha 2}^* + Z_{\alpha 1}^* g'/g)}{m_{\chi_\alpha^e}} h_e^j E_{jl} E_{ml}^* \tilde{A}^{pm} L_{rq} L_{pq}^* \tan \beta \times U_{\beta 2}^* V_{\beta 2}^* m_{\chi_\beta^+} I(m_{\chi_\beta^+}, m_{\tilde{E}_l}, m_{\tilde{L}_q}, m_{H^+}) + (i \leftrightarrow j). \quad (\text{B.33})$$

The second possibility gives

$$(I, IV)_2 = - \sum_{\alpha, m, n} \delta_\mu^i \delta_B^n |\mu| |B| \frac{g}{\sqrt{2}} \frac{Z_{\alpha 3}^* (Z_{\alpha 2}^* - Z_{\alpha 1}^* g'/g)}{m_{\chi_\alpha^e}} m_{e_j} h_e^j \tan \beta L_{jm} L_{nm}^* I(m_{e_j}, m_{\tilde{L}_m}, m_{H^+}) + (i \leftrightarrow j), \quad (\text{B.34})$$

and the third possibility is

$$(I, IV)_3 = \sum_{\beta, \alpha, l, m, p, q, r} \delta_B^r \delta_\mu^i |\mu| |B| \frac{g}{\sqrt{2}} \frac{Z_{\alpha 3}^* Z_{\alpha 3}^*}{m_{\chi_\alpha^e}} h_e^j E_{jl} E_{ml}^* \tilde{A}^{pm} L_{rq} L_{pq}^* \tan \beta \times U_{\beta 2}^* V_{\beta 1}^* m_{\chi_\beta^+} I(m_{\chi_\beta^+}, m_{\tilde{E}_l}, m_{\tilde{L}_q}, m_{H^+}) + (i \leftrightarrow j), \quad (\text{B.35})$$

which reduces, for diagonal  $\tilde{A}, L$  and  $E$  to

$$(I, IV) = - \sum_{\beta, \alpha} \delta_B^j \delta_\mu^i |\mu| |B| \frac{g}{\sqrt{2}} \frac{Z_{\alpha 3}^*}{m_{\chi_\alpha^e}} \left\{ (Z_{\alpha 2}^* + Z_{\alpha 1}^* g'/g) U_{\beta 2}^* V_{\beta 2}^* + Z_{\alpha 3}^* U_{\beta 2}^* V_{\beta 1}^* \right\} \times m_{\chi_\beta^+} h_e^j m_{e_j} (A + |\mu| \tan \beta) \tan \beta I(m_{\chi_\beta^+}, m_{\tilde{E}_j}, m_{\tilde{L}_j}, m_{H^+}) - \sum_{\alpha} \delta_\mu^i \delta_B^j |\mu| |B| \frac{g}{\sqrt{2}} \frac{Z_{\alpha 3}^* (Z_{\alpha 2}^* - Z_{\alpha 1}^* g'/g)}{m_{\chi_\alpha^e}} m_{e_j} h_e^j \tan \beta I(m_{e_j}, m_{\tilde{L}_m}, m_{H^+}) + (i \leftrightarrow j). \quad (\text{B.36})$$

- $R_p$ -violation at I and III (diagram 16, equation A.36)

$$(I, III) = - \sum_{\alpha \beta} \delta_\mu^i \delta_\mu^j |\mu|^2 \frac{g}{\sqrt{2}} \sin^2 \beta h_e^j m_{e_j} \left\{ V_{\alpha 2}^* U_{\alpha 1}^* m_{\chi_\alpha^+} \frac{Z_{\beta 3}^* Z_{\beta 4}^*}{m_{\chi_\beta^e}} + V_{\alpha 2}^* U_{\alpha 2}^* m_{\chi_\alpha^+} \frac{(Z_{\beta 2}^* - Z_{\beta 1}^* g'/g) Z_{\beta 3}^*}{m_{\chi_\beta^e}} \right\} I(m_{e_j}, m_{H^+}, m_{\chi_\alpha^+}) + (i \leftrightarrow j). \quad (\text{B.37})$$

- $R_p$ -violation at III and VIII (diagram 15, equation A.34)

$$(III, VIII) = - \sum_{\alpha\beta,k,l} \delta_\mu^k \delta_\mu^j |\mu|^2 \frac{g}{\sqrt{2}} L_{il}^* L_{kl} h_e^k m_{e_k} V_{\alpha 2}^* U_{\alpha 1}^* m_{\chi_\alpha^+} \frac{Z_{\beta 3}^* Z_{\beta 4}^*}{m_{\chi_\beta^0}} I(m_{e_k}, m_{\tilde{L}_l}, m_{\chi_\alpha^+}) + (i \leftrightarrow j), \quad (B.38)$$

which reduces for diagonal  $L$  to

$$(III, VIII) = - \sum_{\alpha\beta} \delta_\mu^i \delta_\mu^j |\mu|^2 \frac{g}{\sqrt{2}} h_e^i m_{e_i} V_{\alpha 2}^* U_{\alpha 1}^* m_{\chi_\alpha^+} \frac{Z_{\beta 3}^* Z_{\beta 4}^*}{m_{\chi_\beta^0}} I(m_{e_i}, m_{\tilde{L}_i}, m_{\chi_\alpha^+}) + (i \leftrightarrow j). \quad (B.39)$$

- $R_p$ -violation at III and VII in  $g - \lambda$  loop; this is zero of the sleptons are mass-degenerate (diagram 18, equation A.39).

$$(III, VII) = \sum_{\alpha,k,l,m} \delta_\mu^k |\mu| \delta_\lambda^{mjk} \frac{g}{\sqrt{2}} m_{e_k} V_{\alpha 2}^* U_{\alpha 1}^* m_{\chi_\alpha^+} L_{il}^* L_{ml} I(m_{e_k}, m_{\tilde{L}_l}, m_{\chi_\alpha^+}) + (i \leftrightarrow j), \quad (B.40)$$

which for diagonal  $L$  reduces to

$$(III, VII) = \sum_{\alpha,k} \delta_\mu^k |\mu| \delta_\lambda^{ijk} \frac{g}{\sqrt{2}} m_{e_k} V_{\alpha 2}^* U_{\alpha 1}^* m_{\chi_\alpha^+} I(m_{e_k}, m_{\tilde{L}_i}, m_{\chi_\alpha^+}) + (i \leftrightarrow j). \quad (B.41)$$

- $R_p$ -violation at (III, IV) (diagram 14, equation A.32)

$$(III, IV) = - \sum_{\alpha,l,k} \delta_\mu^j \delta_B^k |\mu| |B| \frac{g}{\sqrt{2}} U_{\alpha 1}^* V_{\alpha 2}^* m_{\chi_\alpha^+} m_{e_j} h_e^j L_{il}^* L_{kl} \tan \beta I(m_{e_j}, m_{\tilde{L}_l}, m_{H^+}, m_{\chi_\alpha^+}) + (i \leftrightarrow j), \quad (B.42)$$

which reduces for diagonal  $L$  to

$$(III, IV) = - \sum_{\alpha} \delta_\mu^j \delta_B^i |\mu| |B| \frac{g}{\sqrt{2}} U_{\alpha 1}^* V_{\alpha 2}^* m_{\chi_\alpha^+} m_{e_j} h_e^j \tan \beta I(m_{e_j}, m_{\tilde{L}_i}, m_{H^+}, m_{\chi_\alpha^+}) + (i \leftrightarrow j). \quad (B.43)$$

- (IV, VIII) and (IV, VII) do not exist, because a doublet slepton must come out of II, so no particles carrying lepton number would arrive at VII.
- (IV, V) and (IV, VI) do not exist, because there cannot be two units of lepton number violation on a charged line.
- (V, VIII) and (V, VII) do not exist, because a doublet slepton must come out of II, so no particles carrying lepton number would arrive at VII.

## C. Conventions and Feynman rules

We take all coupling constants to be real. Indices on Yukawa couplings and  $A$  are in order doublet( $d$ ) singlet ( $s$ ):  $h_e^{ds}$ . We work in the mass eigenstate basis of the charged leptons and down-type quarks, where the Yukawa couplings are diagonal and only need one index. In Appendix A, we absorb the slepton and squark mixing matrices into the Yukawa and gauge couplings at the vertices, so they are not diagonal when a scalar meets a fermion.

The MSSM neutralino mass matrix is diagonalised by the matrix  $Z_{mf}$ , with flavour eigenstate index  $f:1..4$  corresponding to  $(-i\tilde{B}, -i\tilde{W}^o, \tilde{h}_u^o, \tilde{h}_d^o)$ . The first index  $m$  is the mass eigenstate index. The chargino mass matrix is diagonalised by matrices  $U$  and  $V$ :  $U^*MV^\dagger = M_{diag}$ , so the positive [negative] mass eigenstates are  $\chi_m^+ = V_{mf}\psi_f^+$  [ $\chi_m^- = U_{mf}\psi_f^-$ ], where  $\psi_f^+ = (-i\tilde{w}^+, \tilde{h}_u^+)$  and  $\psi_f^- = (-i\tilde{w}^-, \tilde{h}_d^-)$ . The doublet and singlet charged slepton (down-type quark) mass matrices are separately diagonalised by matrices  $L_{fm}$  and  $E_{fm}$  ( $Q_{fm}$  and  $D_{fm}$ ), with index order flavour eigenstate–mass eigenstate. We include the  $A$  term mixing between doublets and singlets in perturbation theory. The matrices  $L, E, Q$  and  $D$  do not appear in Appendix A; instead we absorb them into  $\tilde{A}, \tilde{A}_d$  and the gauge and yukawa vertex couplings. We use bold face indices to indicate the squark/slepton mass eigenstates in Appendix A, so

$$\tilde{A}^{\mathbf{l}\mathbf{m}} = L_{pl}^* \tilde{A}^{pq} E_{qm}^*, \quad \tilde{A}_d^{\mathbf{l}\mathbf{m}} = Q_{pl}^* \tilde{A}_d^{pq} D_{qm}^*, \quad h_e^{\mathbf{l}\mathbf{m}} = L_{kl} h_e^{km} \quad (\text{C.1})$$

We also absorb the diagonalisation matrices into the gauge couplings, so  $g$  also appears with indices. Usually

$$g^{i\mathbf{l}} = gL^{i\mathbf{l}} \quad (\text{C.2})$$

however,  $g$  appears in the formulae for diagram 17 having absorbed  $L, E, Q$  or  $D$ .

We use MSSM Feynman rules from [3], with additional Feynman rules to include the  $\mathcal{R}_p$  interactions in figures 3,4 and 5. Line direction is superfield chirality.

For a Lagrangian

$$\mathcal{L} = \bar{\psi}(i\cancel{\partial} - m)\psi, \quad (\text{C.3})$$

we fix the phase of the mass insertion to be  $-i$  because

$$\frac{i}{\not{p} - m} = \frac{i}{\not{p}} + \frac{i}{\not{p}}(-im)\frac{i}{\not{p}} + \dots \quad (\text{C.4})$$

The  $-i\mu_i$  mass insertions on the external legs of the diagram mix the incident flavour eigenstate neutrino  $\nu_i$  with the  $\tilde{h}_u^o$  component of a neutralino. So the external leg propagator delivering a flavour eigenstate neutralino  $f$  to vertex II is:

$$\frac{i}{\not{p}}(-i\mu_i) \sum_{\alpha} \frac{iZ_{\alpha 3}^* Z_{\alpha f}^*}{\not{p} - m_{\chi_{\alpha}^o}} = \frac{i}{\not{p}}(-\mu_i) \sum_{\alpha} \left( \frac{Z_{\alpha 3}^* Z_{\alpha f}^*}{m_{\chi_{\alpha}^o}} \right), \quad (\text{C.5})$$

where we have used  $p^2 = 0$ . This gives the Feynman rules of figure 3.

The  $R_p$  violating  $\mu_i$  and  $B_i$  mass insertions, and the  $R_p$  conserving  $\tilde{A}$  mass insertion, on internal charged lines are negative (by SU(2) antisymmetric contraction), so effectively appear in the amplitude with a negative sign:

$$\frac{i}{\not{p} - m_1}(i|\mu_i|)\frac{i}{\not{p} - m_2} = \frac{i}{\not{p} - m_1} \frac{-|\mu_i|}{\not{p} - m_2}. \quad (\text{C.6})$$

(However, the  $R_p$  part of  $\tilde{A}$  is  $-\lambda^{i4i}\mu_i v_u/\sqrt{2} = m_{e_i}\mu_i \tan\beta$ , so appears positive in the amplitude...).

The Feynman rule we quote in figure 4 for the mass insertion  $B_i$  also includes the effect of the soft mass  $m_{4i}^2$ . The minimisation condition for the potential, in the  $\langle \tilde{\nu}_i \rangle = 0$  basis, implies that  $m_{4i}^2 = -B_i \tan\beta$  (at arbitrary loop order) [19], so the  $R_p$  mixing between  $H^-$  and  $E_L$  is

$$-B_i \cos\beta + m_{4i}^2 \sin\beta = -\frac{B_i}{\cos\beta}. \quad (\text{C.7})$$

## D. Numerical Bounds

We give results for two different values of  $\tan\beta = 2, 10$  whenever necessary. This gives us an indication of the explicit dependence of the bounds of  $\tan\beta$ , although there is another dependence implicit in the neutralino/chargino mixing matrices which we do not address here. Once again, we emphasize that we make the assumptions described in section 4 in order that the combination of couplings constants are allowed the largest possible values. It is easy to see that under these assumptions the integrals that appear in the expressions of appendices A and B can be simply replaced by

$$\begin{aligned} I(m_1, m_2, m_3) &\rightarrow \frac{1}{16\pi^2} \frac{1}{m_{susy}^2}, \\ I(m_1, m_2, m_3, m_4) &\rightarrow \frac{1}{16\pi^2} \frac{1}{m_{susy}^4}, \\ I(m_1, m_2, m_3, m_4, m_5) &\rightarrow \frac{1}{16\pi^2} \frac{1}{m_{susy}^6}. \end{aligned} \quad (\text{D.1})$$

Below for all bounds we use  $|m_\nu|$ .

- Tree-level contribution

$$|m_\nu^{ij}| = \delta_\mu^i \delta_\mu^j m_{susy}, \quad (D.2)$$

which gives the constraint

$$\delta_\mu^i \delta_\mu^j \leq 10^{-12}. \quad (D.3)$$

- Diagram 1

$$m_\nu^{ij} = \frac{1}{8\pi^2} \frac{1}{m_{susy}} \sum_{k,n} \delta_\lambda^{ink} \delta_\lambda^{jkn} m_{e_n} m_{e_k}. \quad (D.4)$$

Using the mass hierarchy of the lepton sector for  $i, j \neq 3$  we get

$$\begin{aligned} \delta_\lambda^{i33} \delta_\lambda^{j33} &\leq 0.1 \text{eV} 8\pi^2 \frac{m_{susy}}{m_\tau^2}, \\ \delta_\lambda^{i33} \delta_\lambda^{j33} &\leq 2.7 \times 10^{-7}, \end{aligned} \quad (D.5)$$

for  $m_{susy} = 100 \text{GeV}$ .

For  $i = 1, 2, j = 3$  and  $j = 1, 2, i = 3$

$$\begin{aligned} \delta_\lambda^{i32} \delta_\lambda^{j23} &\leq 0.1 \text{eV} 8\pi^2 \frac{m_{susy}}{m_\tau m_\mu}, \\ \delta_\lambda^{i33} \delta_\lambda^{j33} &\leq 4.4 \times 10^{-6}, \end{aligned} \quad (D.6)$$

for  $m_{susy} = 100 \text{GeV}$ .

For  $i, j = 3$

$$\begin{aligned} \delta_\lambda^{i22} \delta_\lambda^{j22} &\leq 0.1 \text{eV} 8\pi^2 \frac{m_{susy}}{m_\mu^2}, \\ \delta_\lambda^{i33} \delta_\lambda^{j33} &\leq 7.1 \times 10^{-5}, \end{aligned} \quad (D.7)$$

for  $m_{susy} = 100 \text{GeV}$ . We can summarize the constraints in tables in the following way,

$$\delta_\lambda^{ink} \delta_\lambda^{jkn} = \begin{array}{|c|c|c|c|} \hline i/j & 1 & 2 & 3 \\ \hline 1 & 2.7 \times 10^{-7} & 2.7 \times 10^{-7} & 4.4 \times 10^{-6} \\ \hline 2 & 2.7 \times 10^{-7} & 2.7 \times 10^{-7} & 4.4 \times 10^{-6} \\ \hline 3 & 4.4 \times 10^{-6} & 4.4 \times 10^{-6} & 7.1 \times 10^{-5} \\ \hline \end{array} \quad (D.8)$$

- Diagram 2

$$m_\nu^{ij} = \frac{3}{8\pi^2} \frac{1}{m_{\text{susy}}} \sum_{k,n} \delta_{\lambda'}^{ink} \delta_{\lambda'}^{jkn} m_{d_n} m_{e_k}. \quad (\text{D.9})$$

Using the mass hierarchy of the down quark sector we get,

$$\begin{aligned} \delta_{\lambda'}^{i33} \delta_{\lambda'}^{j33} &\leq 0.1 \text{eV} 8\pi^2 \frac{m_{\text{susy}}}{3m_b^2}, \\ \delta_{\lambda'}^{i33} \delta_{\lambda'}^{j33} &\leq 1.05 \times 10^{-8}, \end{aligned} \quad (\text{D.10})$$

for  $m_{\text{susy}} = 100 \text{GeV}$ .

- Diagram 3

$$m_\nu^{ij} = \frac{g^2}{64\pi^2 \cos^2 \beta} m_{\text{susy}} \delta_B^i \delta_B^j. \quad (\text{D.11})$$

This gives

$$\begin{aligned} \delta_B^i \delta_B^j &\leq 0.1 \text{eV} \frac{64\pi^2 \cos^2 \beta}{g^2 m_{\text{susy}}}, \\ \delta_B^i \delta_B^j &\leq 2.9 \times 10^{-10}, \end{aligned} \quad (\text{D.12})$$

for  $\tan \beta = 2$ .

- Diagram 4

$$m_\nu^{ij} = \sum_k \frac{3h_d^k m_{d_k}^2}{16\pi^2 m_{\text{susy}}} (\delta_\mu^j \delta_{\lambda'}^{ikk} + \delta_\mu^i \delta_{\lambda'}^{jkk}). \quad (\text{D.13})$$

Once again using the fermion mass hierarchy we get,

$$m_\nu^{ij} = \frac{3h_b m_b^2}{16\pi^2 m_{\text{susy}}} (\delta_\mu^j \delta_{\lambda'}^{i33} + \delta_\mu^i \delta_{\lambda'}^{j33}). \quad (\text{D.14})$$

Which gives,

$$(\delta_\mu^j \delta_{\lambda'}^{i33} + \delta_\mu^i \delta_{\lambda'}^{j33}) \leq 0.1 \text{eV} \frac{16\pi^2 m_{\text{susy}}}{3h_b m_b^2}. \quad (\text{D.15})$$

For  $\tan \beta = 2$ ,

$$(\delta_\mu^j \delta_{\lambda'}^{i33} + \delta_\mu^i \delta_{\lambda'}^{j33}) \leq 3.2 \times 10^{-7}. \quad (\text{D.16})$$

For  $\tan \beta = 10$ ,

$$(\delta_\mu^j \delta_{\lambda'}^{i33} + \delta_\mu^i \delta_{\lambda'}^{j33}) \leq 7.2 \times 10^{-8}. \quad (\text{D.17})$$

- Diagram 5

$$m_\nu^{ij} = \frac{m_\tau \tan \beta}{16\pi^2 m_{\text{susy}}} \delta_\lambda^{ij3} \delta_B^3 (m_{e_j} h_e^j - m_{e_i} h_e^i). \quad (\text{D.18})$$

For  $\tan \beta = 2$ ,

$$\delta_\lambda^{ij3} \delta_B^3 = \begin{array}{|c|c|c|c|} \hline i/j & 1 & 2 & 3 \\ \hline 1 & 0 & 3.2 \times 10^{-3} & 1.2 \times 10^{-5} \\ \hline 2 & 3.2 \times 10^{-3} & 0 & 1.2 \times 10^{-5} \\ \hline 3 & 1.2 \times 10^{-5} & 1.2 \times 10^{-5} & 0 \\ \hline \end{array} \quad (\text{D.19})$$

For  $\tan \beta = 10$ ,

$$\delta_\lambda^{ij3} \delta_B^3 = \begin{array}{|c|c|c|c|} \hline i/j & 1 & 2 & 3 \\ \hline 1 & 0 & 1.4 \times 10^{-4} & 5.5 \times 10^{-7} \\ \hline 2 & 1.4 \times 10^{-4} & 0 & 5.5 \times 10^{-7} \\ \hline 3 & 5.5 \times 10^{-7} & 5.5 \times 10^{-7} & 0 \\ \hline \end{array} \quad (\text{D.20})$$

- Diagram 6

$$m_\nu^{ij} = \sum_k \frac{h_e^k m_{e_k}^2}{16\pi^2 m_{\text{susy}}} (\delta_\mu^j \delta_\lambda^{ikk} + \delta_\mu^i \delta_\lambda^{jkk}). \quad (\text{D.21})$$

For  $\tan \beta = 2$ ,

$$(\delta_\mu^j \delta_\lambda^{ikk} + \delta_\mu^i \delta_\lambda^{jkk}) = \begin{array}{|c|c|c|c|} \hline i/j & 1 & 2 & 3 \\ \hline 1 & 2.5 \times 10^{-5} & 2.5 \times 10^{-5} & 2.5 \times 10^{-5} \\ \hline 2 & 2.5 \times 10^{-5} & 2.5 \times 10^{-5} & 2.5 \times 10^{-5} \\ \hline 3 & 2.5 \times 10^{-5} & 2.5 \times 10^{-5} & 1.0 \times 10^{-1} \\ \hline \end{array} \quad (\text{D.22})$$

For  $\tan \beta = 10$ ,

$$(\delta_\mu^j \delta_\lambda^{ikk} + \delta_\mu^i \delta_\lambda^{jkk}) = \begin{array}{|c|c|c|c|} \hline i/j & 1 & 2 & 3 \\ \hline 1 & 5.5 \times 10^{-6} & 5.5 \times 10^{-6} & 5.5 \times 10^{-2} \\ \hline 2 & 5.5 \times 10^{-6} & 5.5 \times 10^{-6} & 5.5 \times 10^{-2} \\ \hline 3 & 5.5 \times 10^{-2} & 5.5 \times 10^{-2} & 2.3 \times 10^{-2} \\ \hline \end{array} \quad (\text{D.23})$$

- Diagram 7

$$m_\nu^{ij} = \frac{\tan \beta \sin^2 \beta}{16\pi^2 m_{\text{susy}}} \delta_\mu^i \delta_\mu^j (m_{e_j}^2 h_e^{j^2} + m_{e_i}^2 h_e^{i^2}). \quad (\text{D.24})$$

For  $\tan \beta = 2$ ,

$$\delta_\mu^i \delta_\mu^j = \begin{array}{|c|c|c|c|} \hline i/j & 1 & 2 & 3 \\ \hline 1 & - & - & 7.1 \times 10^{-4} \\ \hline 2 & - & - & 7.1 \times 10^{-4} \\ \hline 3 & 7.1 \times 10^{-4} & 7.1 \times 10^{-4} & 3.5 \times 10^{-4} \\ \hline \end{array} \quad (\text{D.25})$$

For  $\tan \beta = 10$ ,

$$\delta_\mu^i \delta_\mu^j = \begin{array}{|c|c|c|c|} \hline i/j & 1 & 2 & 3 \\ \hline 1 & - & - & 5.7 \times 10^{-6} \\ \hline 2 & - & 0.35 & 5.7 \times 10^{-6} \\ \hline 3 & 5.7 \times 10^{-6} & 5.7 \times 10^{-6} & 2.8 \times 10^{-6} \\ \hline \end{array} \quad (\text{D.26})$$

The dashed lines mean that there is no bound.

- Diagram 8

$$m_\nu^{ij} = \sum_k \delta_\mu^k m_{e_k} \frac{\tan \beta \sin^2 \beta}{16\pi^2 m_{\text{susy}}} \delta_\lambda^{ijk} (m_{e_j} h_e^j - m_{e_i} h_e^i). \quad (\text{D.27})$$

The bounds can be obtained from the bounds of diagram 5/ $(\sin^2 \beta)$ .

- Diagram 9

$$m_\nu^{ij} = \frac{\tan \beta \sin^2 \beta}{8\pi^2 m_{\text{susy}}} \delta_\mu^i \delta_\mu^j m_{e_i} m_{e_j} h_e^i h_e^j. \quad (\text{D.28})$$

For  $\tan \beta = 2$ ,

$$\delta_\mu^i \delta_\mu^j = \begin{array}{|c|c|c|c|} \hline i/j & 1 & 2 & 3 \\ \hline 1 & - & - & - \\ \hline 2 & - & - & 9.3 \times 10^{-2} \\ \hline 3 & - & 9.3 \times 10^{-2} & 3.5 \times 10^{-4} \\ \hline \end{array} \quad (\text{D.29})$$

For  $\tan \beta = 10$ ,

$$\delta_\mu^i \delta_\mu^j = \begin{array}{|c|c|c|c|} \hline i/j & 1 & 2 & 3 \\ \hline 1 & - & - & - \\ \hline 2 & - & 0.19 & 7.4 \times 10^{-4} \\ \hline 3 & - & 7.4 \times 10^{-4} & 2.8 \times 10^{-6} \\ \hline \end{array} \quad (\text{D.30})$$

- Diagram 10

$$m_\nu^{ij} = \frac{1}{16\pi^2 m_{\text{susy}}} \delta_\mu^i \delta_\mu^j (m_{e_i}^2 h_e^{i^2} + m_{e_j}^2 h_e^{j^2}). \quad (\text{D.31})$$

The bounds here can be obtained from those diagram  $7 \times \tan \beta \sin^2 \beta$ .

- Diagram 11

$$m_\nu^{ij} = \frac{\tan \beta}{16\pi^2 m_{\text{susy}}} \delta_\mu^i \delta_B^j (m_{e_j}^2 h_e^{j^2}) + \delta_\mu^j \delta_B^i (m_{e_i}^2 h_e^{i^2}) \quad (\text{D.32})$$

The bounds here can be obtained from those diagram  $7 \times \sin^2 \beta$ .

- Diagram 12

$$m_\nu^{ij} = \sum_k \frac{m_{e_k}}{16\pi^2 m_{\text{susy}}} \delta_\mu^k \delta_\lambda^{ijk} (m_{e_i} h_e^i - m_{e_j} h_e^j). \quad (\text{D.33})$$

The bounds here can be obtained from those diagram  $5 \times \tan \beta$ .

- Diagram 13

$$m_\nu^{ij} = \frac{1}{8\pi^2 m_{\text{susy}}} \delta_\mu^i \delta_B^j (m_{e_i} h_e^i m_{e_j} h_e^j). \quad (\text{D.34})$$

The bounds here can be obtained from those diagram  $9 \times \tan \beta \sin^2 \beta$ .

- Diagram 14

$$m_\nu^{ij} = \frac{g \tan \beta}{16\pi^2 \sqrt{2}} (\delta_\mu^i \delta_B^j m_{e_i} h_e^i + \delta_\mu^j \delta_B^i m_{e_j} h_e^j). \quad (\text{D.35})$$

For  $\tan \beta = 2$ ,

$$(\delta_\mu^i \delta_B^j) = \begin{array}{c|ccc} i/j & 1 & 2 & 3 \\ \hline 1 & --- & 1.2 \times 10^{-4} & 4.6 \times 10^{-7} \\ 2 & --- & 6.0 \times 10^{-5} & 4.6 \times 10^{-7} \\ 3 & --- & --- & 2.3 \times 10^{-7} \end{array} \quad (\text{D.36})$$

The  $i$  index on  $\delta_\mu$  corresponds to the column, and the  $j$  index to the row, for both the table above and below.

For  $\tan \beta = 10$ ,

$i/j$	1	2	3
1	0.12	$5.3 \times 10^{-6}$	$2.0 \times 10^{-8}$
2	---	$2.6 \times 10^{-6}$	$2.0 \times 10^{-8}$
3	---	---	$1.0 \times 10^{-8}$

(D.37)

- Diagram 15

$$m_\nu^{ij} = \frac{g}{16\pi^2\sqrt{2}}\delta_\mu^i\delta_\mu^j(m_{e_i}h_e^i + m_{e_j}h_e^j). \quad (D.38)$$

The bounds here can be obtained from those diagram  $20 \times \tan \beta \sin^2 \beta$ .

- Diagram 16

$$m_\nu^{ij} = \frac{g \sin^2 \beta}{16\pi^2\sqrt{2}}\delta_\mu^i\delta_\mu^j(m_{e_i}h_e^i + m_{e_j}h_e^j). \quad (D.39)$$

The bounds here can be obtained from those diagram  $20 \times \tan \beta$ .

- Diagram 17

From the slepton-lepton loop, neglecting  $g'$  with respect to  $g$ :

$$m_\nu^{ij} = \sum_k \frac{gm_{e_k}}{16\pi^2\sqrt{2}}(\delta_\mu^i\delta_\lambda^{jkk} + \delta_\mu^j\delta_\lambda^{ikk}) \quad (D.40)$$

$$(\delta_\mu^i\delta_\lambda^{j33} + \delta_\mu^j\delta_\lambda^{i33}) = 1.0 \times 10^{-8} \quad (D.41)$$

From the squark-quark loop:

$$m_\nu^{ij} = 3 \sum_k \frac{gm_{d_k}}{16\pi^2\sqrt{2}}(\delta_\mu^i\delta_\lambda'^{jkk} + \delta_\mu^j\delta_\lambda'^{ikk}) \quad (D.42)$$

$$(\delta_\mu^i\delta_\lambda'^{j33} + \delta_\mu^j\delta_\lambda'^{i33}) = 3.4 \times 10^{-9} \quad (D.43)$$

- Diagram 18

This diagram is non-zero only for non-degenerate sleptons.

- Diagram 19

$$m_\nu^{ij} = \frac{g^2}{64\pi^2 \cos \beta} m_{\text{susy}}(\delta_\mu^i\delta_B^j + \delta_\mu^j\delta_B^i). \quad (D.44)$$

For  $\tan \beta = 2$ ,

$$(\delta_\mu^i \delta_B^j + \delta_\mu^j \delta_B^i) = 6.7 \times 10^{-10} \quad (\text{D.45})$$

For  $\tan \beta = 10$ ,

$$(\delta_\mu^i \delta_B^j + \delta_\mu^j \delta_B^i) = 1.4 \times 10^{-10} \quad (\text{D.46})$$

- Diagram 20

$$m_\nu^{ij} = \frac{g \tan \beta \sin^2 \beta}{16\pi^2 \sqrt{2}} \delta_\mu^i \delta_\mu^j (m_{e_i} h_e^i + m_{e_j} h_e^j). \quad (\text{D.47})$$

For  $\tan \beta = 2$ ,

$i/j$	1	2	3	
$\delta_\mu^i \delta_\mu^j =$	---	$1.5 \times 10^{-4}$	$5.7 \times 10^{-7}$	
1	$1.5 \times 10^{-4}$	$7.5 \times 10^{-5}$	$5.7 \times 10^{-7}$	
2	$5.7 \times 10^{-7}$	$5.7 \times 10^{-7}$	$2.8 \times 10^{-7}$	
3				

(D.48)

For  $\tan \beta = 10$ ,

$i/j$	1	2	3	
$\delta_\mu^i \delta_\mu^j =$	0.12	$5.4 \times 10^{-6}$	$2.0 \times 10^{-8}$	
1	$5.4 \times 10^{-6}$	$2.7 \times 10^{-6}$	$2.0 \times 10^{-8}$	
2	$2.0 \times 10^{-8}$	$2.0 \times 10^{-8}$	$1.0 \times 10^{-8}$	
3				

(D.49)

- Diagram 21

$$m_\nu^{ij} = \frac{g \tan \beta}{16\pi^2 \sqrt{2}} (\delta_\mu^i \delta_B^j m_{e_j} h_e^j + \delta_\mu^j \delta_B^i m_{e_i} h_e^i). \quad (\text{D.50})$$

Here we obtain the same bounds as in diagram 14, but with the indices on  $\delta_\mu$  and  $\delta_B$  inverted; the bound of diagram 14 on  $\delta_\mu^i \delta_B^j$  applies to  $\delta_\mu^j \delta_B^i$  according to this diagram.

## References

- [1] see for example and refs. therein: R.Barbieri, J. Ellis and M.K. Gaillard, Phys. Lett. **B90** (1980) 249; M. Gell-Mann, P. Ramond and R. Slansky, *Proceedings of the Supergravity Stony Brook Workshop*, New York 1979, eds. P. Van Nieuwenhuizen and D. Freedman; T. Yanagida, *Proceedings of the Workshop on Unified Theories and Baryon Number in the Universe*, Tsukuba, Japan 1979, eds. A. Sawada and A. Sugamoto; S. Dimopoulos, L.J. Hall and S. Raby, Phys. Rev.

- Lett. **68** (1992) 1984; G.K. Leontaris et al, Phys. Rev. **D53** (1996) 6381; S. Lola and J. D. Vergados, Prog. Part. Nucl. Phys.**40** (1998) 71; G. Altarelli and F. Feruglio, hep-ph/9905536; G. Altarelli, F. Feruglio, I. Masina *Phys.Lett.* **B472** (2000) 382; J.A. Casas et al, *Nucl. Phys.* **B569** (2000) 82 and *JHEP* **09** (1999) 015; M. Carena et al, *Eur. Phys. J* **C12** (2000) 507; P. Langacker, Nucl. Phys. Proc. Suppl. **77** (1999) 241; Z. Berezhiani and A. Rossi, *JHEP* **9903** (1999) 002.
- [2] for a review, see, *e.g.*, H.P. Nilles, *Phys. Rep.* **110**(1984) 1; R. Barbieri, *Riv. Nuovo Cimento* **11** (1988) 1.
- [3] H.E. Haber and G.L. Kane, *Phys. Rep.* **117**(1985) 75.
- [4] G.R. Farrar and P. Fayet, *Nucl. Phys.*, **B76** (1978) 575.
- [5] Y. Fukuda et al., Super-Kamiokande Collaboration, Phys. Lett. **B 433** (1998) 9; Phys. Lett. **B 436** (1998) 33; Phys.Rev.Lett. **81** (1998) 1562. R. Becker-Szendy et al., IMB Collaboration, Nucl. Phys. **B** (Proc. Suppl.) **38** (1995) 331. W.W.M. Allison et al. Soudan-2 Collaboration, Phys. Lett. **B391** (1997) 491, Phys. Lett. **B449** (1999) 137. Y. Fukuda et al., Kamiokande Collaboration, Phys. Lett. **B 335** (1994) 237. R. Davis et al., Phys.Rev.Lett. **21** (1968) 1205; B.T. Cleveland et al., Astrophys. J. **496** (1998) 505. W. Hampel et al., Phys. Lett. **B 388** (1996) 384. D.N. Abdurashitov et al., Phys. Rev. Lett. **B 77** (1996) 4708; astro-ph/9907131. K. S. Hirata et al., Kamiokande Collaboration, Phys. Rev. Lett. **77** (1996) 1683. Y. Fukuda et al., Super-Kamiokande Collaboration, Phys.Rev.Lett. **81** (1998) 1158.
- [6] H.P. Nilles and N. Polonsky, Nucl. Phys. **B499** (1997) 33. T. Banks, Y. Grossman, E. Nardi and Y. Nir, Phys. Rev. **D52** (1995) 5319. F.M. Borzumati, Y. Grossman, E. Nardi and Y. Nir, Phys.Lett. **B384** (1996) 123. E.Nardi, Phys. Rev. **D55** (1997) 5772.
- [7] L. Hall and M. Suzuki. *Nucl. Phys.*, B231:419, 1984.
- [8] Y. Grossman and H. Haber, *Phys. Rev. Lett.* **78** (1997) 3438; *Phys.Rev.* **D59** 093008; hep-ph/9906310.
- [9] H. Dreiner, hep-ph/9707435. G. Bhattacharyya, Nucl. Phys. Proc. Suppl. **52A** (1997) 83 and hep-ph/9709395. B. Allanach, A. Dedes and H. Dreiner, *Phys. Rev.* **D60** (1999) 075014.
- [10] S. Davidson and J. Ellis, Phys. Lett. **B390** (1997) 210; Phys. Rev. **D56** (1997) 4182. S. Davidson, *Phys. Lett.*, **B439** (1998) 63.
- [11] J. Ferrandis, *Phys. Rev.* **D60** (1999) 095012.
- [12] S. Davidson and M. Losada, *JHEP* 0005 (2000) 021.
- [13] Y. Grossman and H. Haber, hep-ph/0005276.

- [14] L. J. Hall, V.A. Kostelecky, S. Raby, *Nucl.Phys.* **B267** (1986) 415.
- [15] R. Hempfling *Nucl.Phys.* **B478** (1996) 3.
- [16] Eung Jin Chun, Sin Kyu Kang, *Phys.Rev.* **D61** (2000) 075012,
- [17] M. Hirsch, M.A. Diaz, W. Porod, J.C. Romao, J.W.F. Valle, hep-ph/0004115.
- [18] R. Godbole, P. Roy and X. Tata, *Nucl. Phys.* **B401** (1993) 67. M. Nowakowski and A. Pilaftsis, *Nucl. Phys.* **B461** (1996) 19. B. de Carlos and P. White, *Phys. Rev.* **D54** (1996) 3427. A.Y. Smirnov and F. Vissani, *Nucl. Phys.* **B460** (1996) 37. D.E. Kaplan and A.E. Nelson, *JHEP* **01** (2000) 033.. E.J. Chun and J.S. Lee, *Phys. Rev.* **D60** (1999) 075002. V. Bednyakov, A. Faessler and S. Kovalenko, *Phys. Lett.* **B442** (1998) 203. J.C. Romão, hep-ph/9907466. S.Y. Choi, E.J. Chun, S.K. Kang and J.S. Lee, *Phys. Rev.* **D 60** (1999) 075002. M. Dress, S. Pakvasa, X. Tata and T. ter Veldhuis, *Phys. Rev.* **D57** (1997) 5335. S. Rakshit, G. Bhattacharyya and A. Raychadhuri, *Phys. Rev.* **D59** 091701. G. Bhattacharyya, H.V. Klapdor-Kleingrothaus, H. Pas, *Phys.Lett.* **B463** (1999) 77. S. Bergmann, H.V. Klapdor-Kleingrothaus, H. Pas, hep-ph/0004048. E.J. Chun, S.K. Kang, C.W. Kim and J.S. Lee, *Nucl. Phys.* **B544** (1999) 89. K. Choi, E.J. Chun and K. Hwang, *Phys. Rev.* **D60** (1999) 031301. O.C.W. Kong, *Mod. Phys. Lett.* **A14** (1999) 903. E. Ma, *Phys. Rev.* **D61** (2000) 033012. A. Joshipura and S. Vempati, *Phys. Rev.* **D 60** (1999) 111303. A. Joshipura, V. Ravindran and S. Vempati, *Phys. Lett* **B451** (1999) 98; A. Joshipura and M. Nowakowshi, *Phys. Rev.* **D51** (1995) 2421. A. Datta, B. Mukhopadhyaya and S. Roy, *Phys. Rev.* **D61** (2000) 055006. F Takayama, M. Yamaguchi, *Phys.Lett.* **B476** (2000) 116. N. Haba, M. Matsuda, M. Tanimoto, *Phys.Lett.* **B478** (2000) 351-357. B. Mukhopadhyaya, S. Roy, F. Vissani, *Phys.Lett.* **B443** (1998) 191. K. Choi and E.J. Chun, *Phys. Lett.* **B488** (2000) 145. J. Mira, E. Nardi, D. Restrepo and J. Valle, hep-ph/0007266. K. Cheung and O.C.W. Kong, *Phys. Rev.* **D61** (2000) 113012. Kiwoon Choi, Eung Jin Chun, Kyuwan Hwang, *Phys.Lett.***B488** (2000)145-152. hep-ph/0005262
- [19] S. Davidson, M. Losada, N. Rius, *Nucl. Phys.* **B587** 118 (2000), [hep-ph/9911317].
- [20] A. Abada and M. Losada, *Nucl Phys.* **B585** (2000) 45, [hep-ph/9908352].
- [21] A. Abada and M. Losada, *Phys. Lett.* **B492** 310 (2000), [hep-ph/0007041].
- [22] O.C.W. Kong, *JHEP* 0009 (2000) 037.
- [23] S. Davidson and S. King, *Phys. Lett.* **B445** (1998) 191.
- [24] A.Abada, S. Davidson, M. Losada, work in progress.

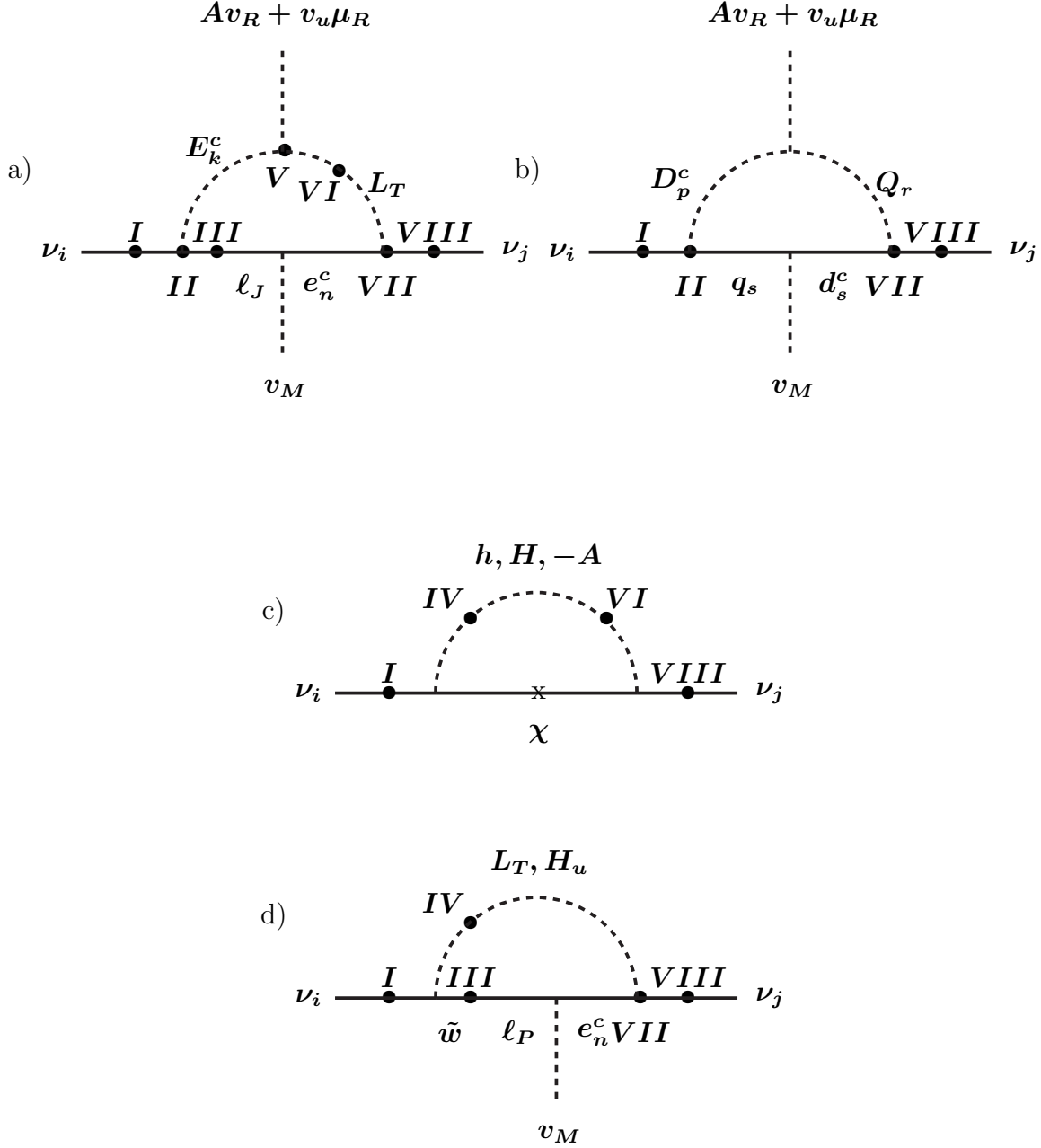


**Figure 2:** Schematic representation of one-loop diagrams contributing to neutrino masses, in a Lagrangian basis. The blobs indicate possible positions for  $\mathcal{R}_p$  interactions, which can be trilinears (at positions II and VII) or mass insertions. The misalignment between  $\vec{\mu}$  and  $\vec{v}$  allows a mass insertion on the lepton/higgsino lines (at points I, III, or VIII) and at the  $A$ -term on the scalar line (position V). The soft  $\mathcal{R}_p$  masses appear as mass insertions at positions VI and IV on the scalar line. Figure a) is the charged loop with trilinear couplings  $\lambda$  (or  $h_e$ ) at the vertices. Figure b) is the coloured loop with trilinear  $\lambda'$  or yukawa  $h_b$  couplings. Figure c) is the neutral loop with two gauge couplings (in the MSSM mass eigenstate basis), and figure d) is the charged loop with one gauge and and a Yukawa coupling. This diagram occurs if gauginos mix with charged leptons—that is if  $\delta_\mu \neq 0$ .

$$\begin{aligned}
\nu_i \text{---} \begin{array}{c} \mu_i \\ \text{---} \text{X} \text{---} \\ \tilde{h}_u \\ \text{---} \text{X} \text{---} \\ m_{\chi_\alpha^o} \end{array} \text{---} \tilde{h}_d &= \nu_i \text{---} \begin{array}{c} \mu_i \\ \text{---} \text{X} \text{---} \end{array} \text{---} \tilde{h}_d & -\mu_i \frac{Z_{\alpha 4}^* Z_{\alpha 3}^*}{m_{\chi_\alpha^o}} \\
\nu_i \text{---} \begin{array}{c} \mu_i \\ \text{---} \text{X} \text{---} \\ \tilde{h}_u \\ \text{---} \text{X} \text{---} \\ m_{\chi_\alpha^o} \end{array} \text{---} \tilde{w}^o &= \nu_i \text{---} \begin{array}{c} \mu_i \\ \text{---} \text{X} \text{---} \end{array} \text{---} \tilde{w}^o & -\mu_i \frac{Z_{\alpha 3}^* Z_{\alpha 2}^*}{m_{\chi_\alpha^o}} \\
\nu_i \text{---} \begin{array}{c} \mu_i \\ \text{---} \text{X} \text{---} \\ \tilde{h}_u \\ \text{---} \text{X} \text{---} \\ m_{\chi_\alpha^o} \end{array} \text{---} \tilde{b}^o &= \nu_i \text{---} \begin{array}{c} \mu_i \\ \text{---} \text{X} \text{---} \end{array} \text{---} \tilde{b}^o & -\mu_i \frac{Z_{\alpha 3}^* Z_{\alpha 1}^*}{m_{\chi_\alpha^o}}
\end{aligned}$$

**Figure 3:** Feynman rules for mass insertions on external legs. The left hand column is a more correct representation; we use the abbreviated notation of the central column in figure 2.

$$\begin{aligned}
\tilde{h}_d \text{---} \begin{array}{c} \mu_i \\ \text{---} \text{X} \text{---} \\ \tilde{h}_u \end{array} & i\mu_i \\
H^+ \text{---} \begin{array}{c} B_i, m_{4i}^2 \\ \text{---} \text{X} \text{---} \\ E_L \end{array} & i \frac{B_i}{\cos \beta} \\
H^- \text{---} \begin{array}{c} \tilde{A} \\ \text{---} \text{X} \text{---} \\ E^c \end{array} & -i \sum_k \mu_k (m_{e_k} \tan \beta) \sin \beta
\end{aligned}$$

**Figure 4:** Internal charged line mass insertions.

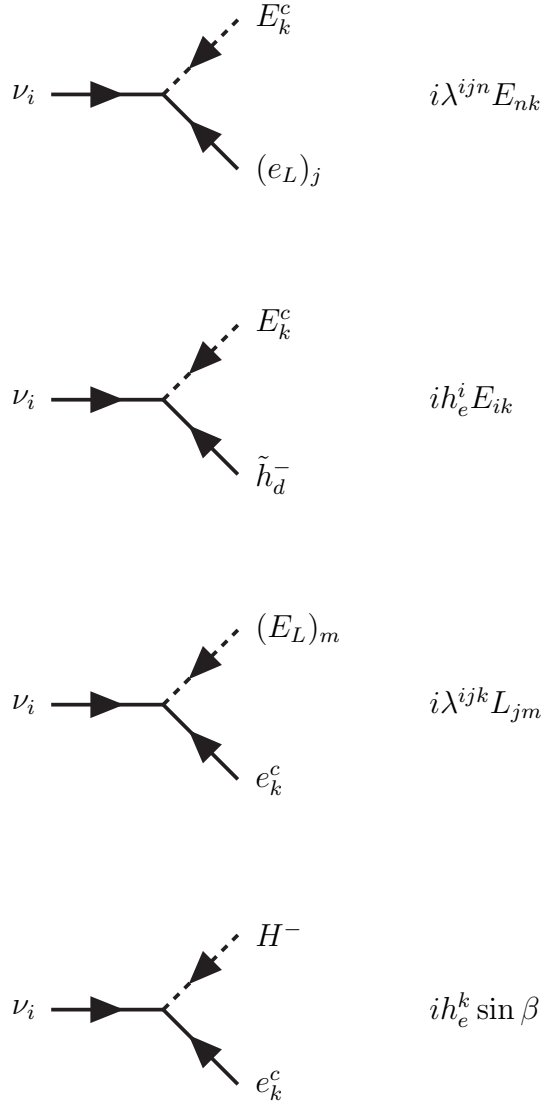


**Figure 5:** Feynman rules for trilinear/Yukawa interactions. For the quarks, replace  $\lambda_{ijk} \rightarrow \lambda'^{ijk}$ ,  $E_k^c \rightarrow D_k^c$ ,  $(e_L)_j \rightarrow (q_L)_j$ , and so on.